Assessment of MODIS BRDF shape indicators

JIAO Ziti , LI Xiaowen , WANG Jindi , ZHANG Hu

State Key Laboratory of Remote Sensing Science, *Jointly Sponsored by Beijing Normal University and the Institute of Remote Sensing Applications of Chinese Academy of Sciences*, *School of Geography*, *Beijing Normal University*, *Beijing Key Laboratory of Environmental Remote Sensing and Digital City*, *Beijing* 100875, *China*

Abstract: Bidirectional Reflectance Distribution Function (BRDF) shape indicators of Moderate Resolution Imaging Spectroradiometer (MODIS) are among MODIS BRDF/Albedo products and are helpful in expanding the application of BRDF remote sensing data. This paper evaluates the MODIS BRDF shape indicators with the statistical analysis methods by using various collected ground BRDF datasets and MODIS products. Our result presents several major findings: (1) the MODIS BRDF shape indicators contain the information regarding 3-D structure of land surface and have the possibility to retrieve the structural parameters of the land surface; (2) the MODIS BRDF shape indicators are intrinsically three-dimensional. Since Anisotropic Index (ANIX) is highly related to Anisotropic Factor (ANIF) and has wider value range than the ANIF, the ANIF may be removed from the MODIS BRDF shape indicator products for refinement of the MODIS BRDF/Albedo products; (3) Anisotropic Flat Index (AFX) is related to basically scattering types of land surface with low within-class variances, so it is considered to be more useful in improving land cover classification accuracy.

Key words: MODIS, BRDF, BRDF shape indicators, vegetation structure, vegetation index

CLC number: TP701 **Document code:** A

Citation format: Jiao Z T, Li X W, Wang J D and Zhang H. 2011. Assessment of MODIS BRDF shape indicators. *Journal of Remote Sensing*, **15**(3): 432–456

1 INTRODUCTION

Over years, a large number of measurements and modeling activities have confirmed the truth of the anisotropic reflectance of the Earth's surface represented by BRDF (Bidirectional Reflectance Distribution Functions). The BRDF is defined as a function of illumination and view geometry for surface scattering in a given band (Nicodemus, *et al*., 1977). A BRDF model relates the bidirectional reflectance to spectral and structural properties of land covers, as a result, the pattern of radiation leaving land surface can be determined in the forward mode by specifying the characteristics of the incident radiation and those of the land cover. Such models provide an opportunity to infer information about the physical parameters of the land cover in the inverse mode.

There are possible three major methods to infer surface structures in terms of land surface anisotropic patterns (Gao, *et al*., 2003): the first method is to directly use the physical BRDF models to retrieve the surface parameters such as vegetation structure with inversion techniques. It is, however, not operationally feasible to do this through such a technique, since the physical BRDF models normally have complicated nonlinear properties, and the inversion requires many highly accurate observations or *a priori* knowledge. Therefore, a variety of multi-angle satellite sensors such as POLDER (Polarization and Directionality of the Earth's Radiation instrument), MODIS (MODerate Resolution Imaging Spectroradiometer), and MISR (Multi-Angle Imaging Spectroradiometer) all use semi-empirical BRDF models as the main algorithm to generate the operational BRDF and albedo products. The semi-empirical, kernel-driven BRDF models have linear forms with several empirical functions (kernels) that are derived through the use of some simplified assumptions. It is kernel weight coefficients that are directly retrieved from such models, instead of the surface structural parameters. However, the expressions of these weight coefficients contain information regarding surface structure parameters (Roujean, *et al*., 1992; Wanner, *et al*., 1995), and therefore provide an opportunity to infer surface structure parameters. This provides us the second method to estimate surface structural parameters from surface anisotropic reflectance patterns (Roujean, *et al*., 1997; Gao, *et al*., 2003).

The third method is usually to construct BRDF shape indicators with reflectance values in typical scattering angles (such as hotspot, dark spot and the zenith), and then the relationship between surface structures and BRDF shape indicators is investigated. Sandmeier, *et al*. (1998, 1999) designed ANIF (ANIsotropy Factor), ANIX (ANI-

Received: 2010-03-05; **Accepted:** 2010-09-30

Foundation: Partly supported by NSFC (No.40871193), National Basic Research Program of China (No. 2007CB714402-8) and Special Foundation for Free Exploration of State Laboratory of Remote Sensing Science (No. 610ZY-06).

First author biography: JIAO Ziti (1970—), male, Associate Professor, Graduated from Department of Geography and Environment at Boston University. His research interests include modeling reflectance anisotropy and albedo, and differentiating land covers with multiple-view-angle remotely sensed data. He has published dozens of papers in several journals. E-mail: jiaozt@bnu.edu.cn

sotropy Index) and NDAX (Normalized Difference Anisotropy indeX). The physical mechanism of hyper-spectral BRDF effect was analyzed with two typical structural vegetations (grass and watercress), showing that these indexes are related to vegetation structures and land cover types. They then investigated roles that these indexes play in discrimination of land covers by applying them to a classification excise over a boreal forest region and concluded that these indexes can improve classification accuracies for certain class, but are inconsistent for all land cover types.

The MODIS BRDF shape indicators are among the operational MODIS BRDF/Albedo products, and are mainly constructed through the use of MODIS BRDF parameters and MODIS forward-modeled reflectances. Although ANIF, ANIX and AFX (Anisotropic Flat indeX) are band-dependent indicators, they are currently generated in red and NIR (Near InfraRed) bands in the operational MODIS BRDF/Albedo products. NDAX is the normalized difference anisotropic index in red and NIR bands. SSI (Structural Scattering Index) is empirically constructed through the combination of volumetric parameters in NIR band and geometric optical parameters in red band (Gao, *et al*., 2003). Among the MODIS BRDF shape indicators, SSI has been explored and validated with ground measurements, as well as satellite samples from MODIS and MISR, showing that SSI is related to the vegetation structures and land cover types. AFX has an equation derived from the kernel-driven BRDF model (Eq. (2)) and is especially appropriate for the description of the MODIS anisotropic reflectance.

The 1st part of the paper provides a comprehensive assessment of MODIS BRDF shape indicators using a variety of ground measurements and four MODIS land products. The 2nd part formulates MODIS BRDF shape indicators. The 3rd part mainly describes datasets used in this study. The 4th part focuses on the analysis of the MODIS BRDF shape indicators with ground measurements, and the 5th part analyzes the MODIS BRDF shape indicators with satellite observations from MODIS. Conclusions and discussion are given in the last part.

2 FORMULATING BRDF SHAPE INDICATORS

The semi-empirical kernel-driven BRDF models adopt linear form and comprise three basic scattering types: isotropic scattering, volumetric scattering and geometric-optical scattering. In the operational MODIS BRDF/Albedo main algorithm, the volumetric scattering and geometric-optical scattering are respectively described by Ross-Thick kernel and Li-Sparse-Reciprocal kernel (henceforth named RTLSR algorithm). They generally have following form (Roujean, *et al*., 1992, Wanner, *et al*., 1995, Lucht, *et al*., 2000).

$$R(\theta,\vartheta,\phi,\Lambda)=f_{\mathrm{iso}}(\Lambda)+f_{\mathrm{vol}}(\Lambda)K_{\mathrm{vol}}(\theta,\vartheta,\phi)+f_{\mathrm{geo}}(\Lambda)K_{\mathrm{geo}}(\theta,\vartheta,\phi) \quad (1)$$

where f_{iso}, f_{vol} and f_{geo} are the spectrally dependent model parameters. K_{geo} and K_{vol} are trigonometric functions of view zenith θ, illumination zenith ϑ and relative azimuth ϕ, providing shapes for surface-scattering and volume-scattering BRDF; f_{iso} is a constant for isotropic scattering; f_{vol} and f_{geo} are constants that weight two BRDFs; $R(\theta,\vartheta,\phi,\Lambda)$ is bidirectional reflectance distribution function in waveband Λ.

A linear regression technique was firstly used to fit available observations and to retrieve the optimal BRDF parameters, and then directional reflectance for any view and solar geometry can be forward modeled through the extrapolation or interpolation of kernel functions. Kernels are trigonometric functions regarding view and illumination geometry and can be pre-calculated, and therefore it is not difficult to calculate black-sky albedo and white-sky albedo by multiplying the pre-integrated kernels by corresponding weighted parameters. As semi-empirical models, kernel-driven BRDF models have merits of empirical model. *i.e*. conciseness, high-speed and strong ability to fit data, and are able to deal with large amount of observations from the EOS (Earth Observing System). Meanwhile, the geometric-optical kernel and the volumetric kernel are of some physical meanings, which could explain and control the extrapolating results over the direction without observations.

MODIS BRDF shape indicator products include five indexes, whose formulas are shown in Table 1.

Table 1 Formulating MODIS BRDF shape indicators

Names	Abbr.	Formulas
Anisotropic factor	ANIF	$\mathrm{ANIF}(\Lambda)=\frac{R_{\_\mathrm{nad}}(\Lambda)}{R_{\_45\mathrm{fw}}(\Lambda)}$
Anisotropic index	ANIX	$\mathrm{ANIX}(\Lambda)=\frac{R_{\_45\mathrm{bw}}(\Lambda)}{R_{\_45\mathrm{fw}}(\Lambda)}$
Normalized difference anisotropic index	NDAX	$\mathrm{NDAX}=\frac{\mathrm{ANIXR}-\mathrm{ANIXN}}{\mathrm{ANIXR}+\mathrm{ANIXN}}$
Structural scattering index	SSI	$\mathrm{SSI}=\ln\left(\frac{f_{\_\mathrm{vol}\_\mathrm{NIR}}}{f_{\_\mathrm{geo}\_\mathrm{red}}}\right)$
Anisotropic flat index	AFX	$\mathrm{AFX}=\frac{\mathrm{WSA}(\Lambda)}{f_{\_\mathrm{iso}}(\Lambda)}$

where $R_{\_\mathrm{nad}}$ refers to the nadir view reflectance; $R_{\_45\mathrm{fw}}$ and $R_{\_45\mathrm{bw}}$ refer to 45° forward and backward reflectances at 45° solar zenith angle; ANIXR and ANIXN refer to red and NIR ANIX; $f_{\_\mathrm{vol}\_\mathrm{NIR}}$ and $f_{\_\mathrm{geo}\_\mathrm{red}}$ are volumetric and geometric-optical parameters in NIR and red bands; $f_{\_\mathrm{iso}}$ is the isotropic parameter. WSA is white sky albedo. *i.e*. bi-hemispherical reflectance.

Based on the RTLSR BRDF model, we derive the AFX as Eq. (2):

$$\mathrm{AFX}(\Lambda)=1+\frac{f_{\mathrm{vol}}(\Lambda)}{f_{\mathrm{iso}}(\Lambda)}\times 0.189184-\frac{f_{\mathrm{geo}}(\Lambda)}{f_{\mathrm{iso}}(\Lambda)}\times 1.377622 \quad (2)$$

where constant 0.189184 and 1.377622 are the bi-hemispherical integral of the Ross Thick kernel and reciprocal LiSparse kernel.

From Eq. (2), we can see that AFX is a linear sum of the volumetric parameter and geometric-optical parameter normalized by isotropic parameter, and weighted by corresponding bi-hemispherical integral of the Ross Thick kernel and the LiSparse-Reciprocal kernel respectively. AFX varies as the geometric-optical and volumetric parameters. If the volumetric scattering effect is greater than the geometric-optical effect, then an AFX > 1 is expected; if the geometric-optical effect is greater than volumetric effect, then an AFX <1 is expected; otherwise, an AFX≈1 is available. Investigation of the shape of RossThick and LiSparse-Reciprocal kernels (Fig. 1) shows that reciprocal LiSparse kernel presents dome-

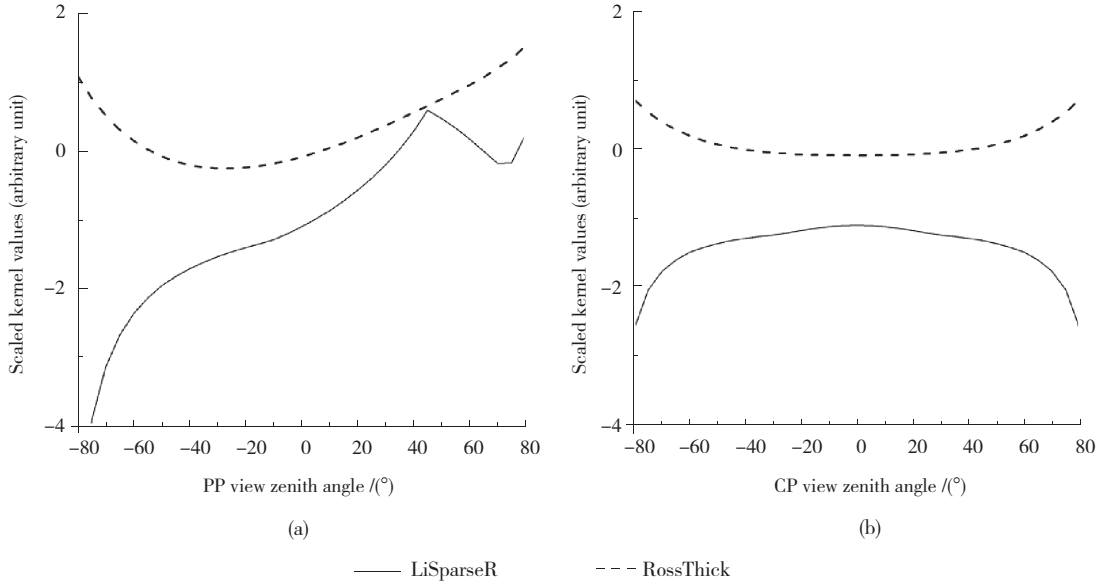

Fig. 1 (a) Principal plane (PP); (b) cross-principal plane (CP) plots of the RossThick (upper curves) and LiSparse-R (lower curves) BRDF model kernel values (the RossThick kernel values were multiplied by 2 for better plotting. The sun is located at positive zenith angles of 45° solar zenith angle. The parameter h/b of the LiSparse-R kernel was set to 2.0 and the parameter b/r to 1.0 as is used in MODIS)

shaped BRDF curve with prominent peak reflectance (hotspot) in retro-solar direction, while the RossThick kernel presents typical bowl-shaped BRDF curve where reflectance near nadir are lower than for larger scattering angle with the minimum usually displaced towards the forward scattering direction. We will explore such a property captured by the AFX through the further analysis of field datasets and MODIS samples in following two sections.

3 DATASETS USED IN THIS STUDY

3.1 Ground BRDF datasets

A number of investigators have collected high-quality ground-based BRDF data sets that cover a large variety of land cover types including barren soil with different roughness, sparsely vegetated grass, grass-like or broadleaf crops, and forest. All ground measurements cover several solar zenith angles. These datasets are summarized as Table 2. The kernel-driven BRDF model was first used to fit ground measurements for retrieval of the three parameters, with which the MODIS BRDF shape indicators were then calculated. Most ground datasets used in this study were used to validate semi-empirical kernel-driven BRDF models (Hu, *et al*., 1997).

3.2 MODIS datasets

Four MODIS land products are used in this study, including MODIS BRDF/Albedo products (Schaaf, *et al*., 2002), MODIS land cover products (Friedl, *et al*., 2003), MODIS vegetation continuous field products (Defries, *et al*., 2000), and MODIS global land cover dynamic products (Zhang, *et al*., 2003).

It is necessary to use a high-quality and pure land cover types to explore MODIS BRDF shape indicators. This would reduce the uncertainty caused by sub-pixel clouds and mixture pixels. To benefit from both MODIS land cover products and MODIS VCF (Vegetation Continuous Field) products, the intersection between these two products was designed to extract some pure IGBP (International Geosphere-Biosphere Programme) classes, and then the band-depend quality flags in MODIS BRDF/Albedo products are used as constraints, so that the best-quality pixels in MODIS BRDF/Albedo products are finally acquired.

In this study, three constraints were used to extract high quality samples from the MODIS BRDF/Albedo products: (1) the highest priority is first given to MODIS BRDF/Albedo quality flags to ensure that the selected samples are the most reliable. Here, 0 flag indicates that the selected pixels have the best quality among the MODIS BRDF/Albedo products; (2) the VCF values corresponding to the selected samples are greater than 70%; (3) the confidence values of IGBP types have high levels in the MODIS land cover products. Through the use of the three constraints above and by further re-sampling two core types (Cropland and Evergreen needleleaf forest) in the study region, the number of the selected samples for each of seven land cover types are approximately confined to 100 pixels (Table 3).

4 ANALYSIS WITH GROUND BRDF DATASETS

4.1 Calculating BRDF shape indicators with ground datasets

Based on the reciprocal RossThick-LiSaprse BRDF model (RTLSR), we first use AMBRALS program to retrieve model BRDF parameters for 20 ground BRDF datasets. The AMBRALS are a set of semi-empirical kernel-driven BRDF models that comprise multiple kernel functions. The operational MODIS RTLSR model is a pair of kernel-function combination among the AMBRALS program. MODIS BRDF shape indicators are then calculated directly with model-retrieved parameters or with the typical

Table 2 Summary of physical characteristics of the field datasets

Code	Cover Type	Cover Type	SZA range /(°)	Cover /%	LAI (green)	Roughness-height /cm	Description	Source
S1	Soil	Alkali flat	NA	Zero	Zero	NA	White	Deering, *et al*. 1990
S2		Smooth	36—53	Zero	Zero	1.2±0.2	Soil Moisture 5.5%; Albedo 19.725%	Irons, 1992
S3		Intermediate	16—52	Zero	Zero	2.6±0.4	Soil Moisture 4.9%; Albedo 17.23%	Irons, 1992
S4		Rough	28—54	Zero	Zero	3.9±0.7	Soil Moisture 4.25%; Albedo 21.375%	Irons, 1992
S5		Ploughed field	26,30,45	Zero	Zero	Depth=8.0 cm		Kimes, 1985
GA	Grassland	Annual	28—50	<5	NA	<3		Kimes, 1985
GO		Orchard grass	45—82	50	1.1	NA		Kimes,1983
GS		Steppe	27—63	18 (20% green)	NA	38	Individual clump cover — 70%	Kimes, 1985
GL		Lowland sedge	53—69	NA	Near zero	NA	Senescent vegetation	Vierling, 1995
GNT		Non-woody tussock	47—75	NA	NA	NA	Mix of standing dead and green	Vierling, 1995
GWT		Woody tussock	49—75	NA	NA	NA	Mix of standing dead, green and emergent deciduous shrub foliage	Vierling, 1995
CUW	Crop	Unirrigated hard wheat	27—51	14 (95% green)	NA	46		Kimes, 1985
CIW		Irrigated wheat	26—59	70	NA	76	Within 15 days of harvest	Kimes, 1985
CC		Corn	23—68	25	0.65	33	Juvenile corn with tilled soil	Kimes,1983
CS1		Soybean	20—49	72	3.0	NA	Canopies incomplete with well define rows	Ranson, 1985
CS2		Soybean	21—38	83	3.9	NA	Canopies incomplete with well defined rows	Ranson, 1985
FS	Forest	Shinnery oak	31—71	60.2	1.75	43	Open canopy dwarf forest with dark leaf litter understorey	Deering, 1992
OJP		Old jack pine	35—73	61*	2.2—2.6	NA	Light coloured reindeer moss understorey ground cover	Deering, 1999
OBS		Old black spruce	35—70	55	3.7—4.0	NA	Understorey of young black spruce	Deering, 1999
ASP		Aspen	41—65	89*	5.5	NA	Mature aspen, hazelnut under-storey	Deering, 1999

* indicates canopy closure percentage

Table 3 Sampled MODIS pixels for each of seven candidate classes

land cover types	Class code	Confidence Level /%	Total pixel /num.	Selected pixel /num.
Evergreen needleleaf forest	ENF	=100	3516	101
Mixed forest	MF	=100	144	144
Open shrubland	OS	⩾76	101	101
Woody savanna	WS	⩾83	100	100
Grassland	GL	⩾99	143	143
Cropland	CL	=100	14520	101
Cropland and natural vegetation mosaic	CNVM	⩾97	119	119

reflectances that are forward calculated with model parameters. A RMSE (Root Mean Square Error) indicates if the fitting is good or not. The RMSE is expressed as Eq. (3).

$$e^2 = \frac{1}{N - n_p} \sum_{j=1}^{N} \frac{(R_j^{\text{obs}} - R_j^{\text{model}})^2}{W_j} \quad (3)$$

where N is observation number, n_p is the parameter number, R^{obs} and R^{model} are the observed and modeled reflectances respectively and W_j is a weighing factor for the j^{th} observations in given band. Here W_j is unity, implying that all observations are of equal importance.

The RMSE values of 20 ground datasets are approximately 0.0142 and 0.0312 respectively in the red and NIR bands, and are apparently less than 0.1 threshold that was defined by the operational MODIS BRDF/Albedo band-dependent quality flags (Jin, *et al*., 2003; Shuai, *et al*., 2008), indicating that RTLSR model fits the ground datasets well. In addition, for vegetation, absolute RMSE values in NIR band is obviously greater than that in red band, while their relative RMSE values in these two bands are very close. This may be related to the reflectance magnitude of vegetation canopy in red and NIR bands, and as well as band-dependent fitting ability of BRDF model in red and NIR bands.

We calculated the MODIS BRDF shape indicators that vary as land cover types for 20 ground measurements (Fig. 2). The Comparison of ANIF and ANIX in Fig. 2 shows an ANIX > ANIF > 1 in both red and NIR bands. This indicates the common characteristic of BRDF shapes captured by 20 ground BRDF shapes. *i.e*. $R_{\_45\text{bw}} > R_{\_\text{nad}} > R_{\_45\text{fw}}$ (Table 1). In other word, these 20 BRDF shapes are all with backward reflectance greater than forward reflectance. However, ANIF and ANIX do not indicate a specific BRDF shape (dome vs. bowl). As a consequence, the reflectance-based BRDF shape indicators may contain information content about anisotropic reflectance pattern of land surface, but have limitation in identifying the specific BRDF shape (dome vs. bowl). The previous study about ANIF and ANIX mainly focuses on the analysis of physical mechanism of the hyper-

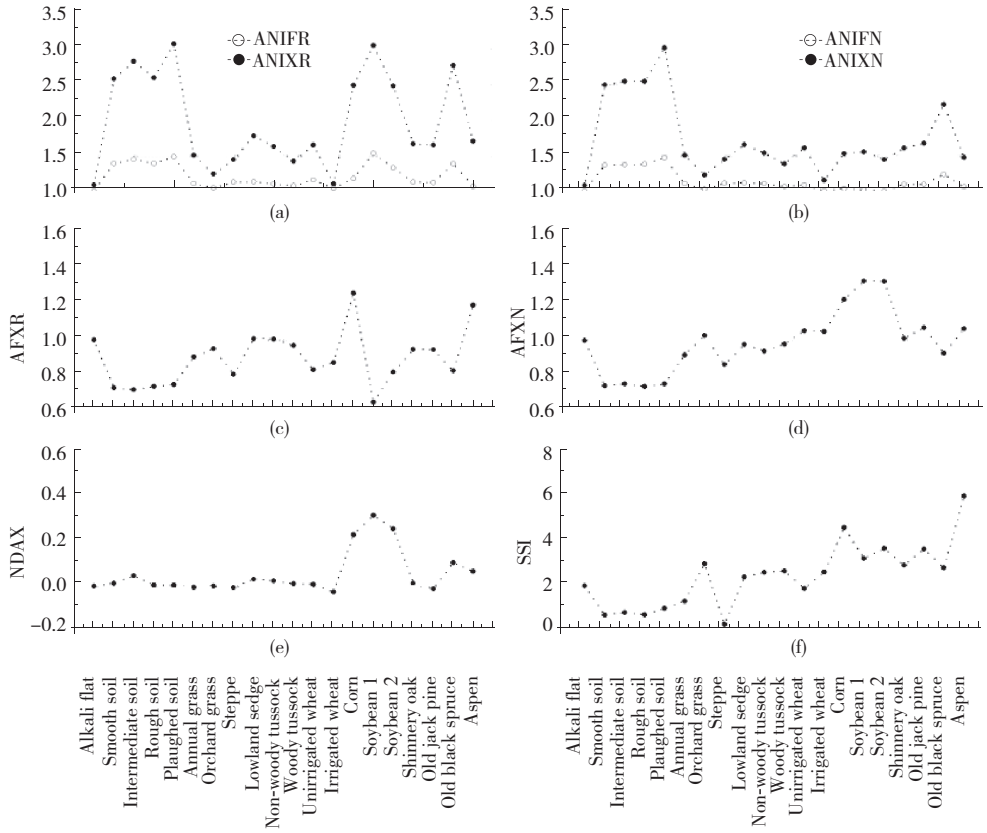

Fig.2 8 MODIS BRDF shape indicators are calculated for 20 ground datasets in red and NIR bands
(Plot (a), (b), (c), (d), (e) and (f) have common x-axis, representing 20 BRDF datasets)

spectral BRDF effects, instead of the analysis of their ability to indicate specific BRDF shape.

Close inspection of AFX curves in Fig. 2, we can see that the AFX values vary around unity and are actually determined by basic scattering types: volumetric scattering and geometric-optical scattering. The further analysis of the relationship between BRDF shape and basic scattering types will be followed. NDAX and SSI do not indicate BRDF shape well for specific band since they are combined from both red and NIR bands.

4.2 Analysis of the model-retrieved parameters

As mentioned above, MODIS BRDF shape indicators rely on the semi-empirical kernel-driven BRDF models, and therefore, it is helpful to understand the MODIS BRDF shape indicators by further analyzing the model parameters for 20 ground measurements. Mean, variance and coefficient of variation (COV) are calculated for these ground measurements (Table 4).

Table 4 Statistical values for volumetric and geometric-optical parameters of ground measurements in red and NIR bands

Parameter	Mean	Var.	COV
VOL_Red	0.0601	0.0527	0.8759
GEO_Red	0.0248	0.0271	1.0928
VOL_NIR	0.1869	0.1202	0.6433
GEO_NIR	0.0303	0.0324	1.0673

From Table 4, we can see that the geometric-optical parameters are very close in red and NIR bands, but the volumetric parameters are obviously greater than the geometric-optical parameters in these two bands. The coefficients of variation for the geometric-optical parameters are also greater than for the volumetric parameters. According to the statistical results, we realized that the volumetric parameters are obviously dominant in NIR band, while volumetric and geometric-optical parameters are very close in red band. For basic scattering types of kernel-driven BRDF model, the volumetric scattering usually represents multiple scattering caused by within-crown gaps, and the geometric-optical scattering usually represents the surface scattering caused by between-crown gaps. The fact that the mean of the geometric-optical parameters are greater than that of the volumetric parameters may imply that there exist significantly different gap distributions within crown and between crowns, which in turn implies different structures for land cover.

We calculated coefficients of determination (R^2) between the volumetric and geometric-optical parameters (Table 5). From Table 5, we can see that the R^2 of the geometric-optical parameters between red and NIR bands is 0.84, but R^2 of the volumetric parameters between these two bands is only 0.022. This shows that the volumetric parameters in red and NIR bands provide more independent information, and are therefore more useful in analyzing land surface properties. For single band parameters, we can see that the geometric-optical parameters are more related to the volumetric parameters in red band ($R^2 \approx 0.6$), but these two parameters are nearly independent of each other ($R^2 \approx 0.083$) in NIR band. This

shows that the volumetric and geometric-optical parameters in NIR band provide relatively independent information as compared with red band, and are therefore more useful in analyzing land surface properties.

Table 5 Coefficients of determination (R^2) for volumetric and geometric-optical parameters in red and NIR bands

	VOL_Red	GEO_Red	VOL_NIR	GEO_NIR
VOL_Red	1.0000	—	—	—
GEO_Red	0.5856	1.0000	—	—
VOL_NIR	0.0220	0.0054	1.0000	—
GEO_NIR	0.5795	0.8435	0.0833	1.0000

4.3 Correlation between MODIS BRDF shape indicators

We calculate the coefficients of determination (R^2) for the MODIS BRDF shape indicators to determine whether there is obvious between-index information redundancy. Table 6 shows the R^2 between all candidate indicators. As can be seen from Table 6, for specific band, ANIF is obviously related to other indicators. For example, for given band, R^2 between ANIF and AFX are about 0.5—0.65. For the specific band, the ANIF is highly related to ANIX with the R^2 greater than 0.9, showing that the there exists obvious redundancy between them. As a result, we propose to remove ANIF from the MODIS BRDF shape indicator products, which could not significantly affect their practical application.

Table 6 Coefficients of determination (R^2) between MODIS BRDF shape indicators

	ANIFR	ANIFN	ANIXR	ANIXN	AFXR	AFXN	NDAX	SSI
ANIFR	1.000	—	—	—	—	—	—	—
ANIFN	0.435	1.000	—	—	—	—	—	—
ANIXR	0.916	0.387	1.000	—	—	—	—	—
ANIXN	0.607	0.944	0.592	1.000	—	—	—	—
AFXR	0.501	0.267	0.229	0.274	1.000	—	—	—
AFXN	0.027	0.659	0.007	0.429	0.104	1.000	—	—
NDAX	0.221	0.078	0.323	0.007	0.000	0.519	1.000	—
SSI	0.096	0.374	0.015	0.235	0.475	0.542	0.216	1.000

Table 7 Coefficients of determination (R^2) between MODIS BRDF shape indicators and NDVI

	ANIFR	ANIFN	ANIXR	ANIXN	AFXR	AFXN	NDAX	SSI
NDVI	0.012	0.325	0.001	0.175	0.200	0.589	0.366	0.829

4.4 Correlation between MODIS BRDF shape indicators and spectral index

We calculated the R^2 between MODIS BRDF shape indicators and NDVI (Normalized Difference Vegetation Index) to analyze the information content of MODIS BRDF shape indicators relative to NDVI. The NDVI can be constructed by normalizing the difference between red and NIR bands, and is usually used to measure the vegetation photosynthetic capacity. The NDVI is as Eq. (4):

$$\mathrm{NDVI} = (R_{\mathrm{NIR}} - R_{\mathrm{red}}) / (R_{\mathrm{NIR}} + R_{\mathrm{red}}) \quad (4)$$

where R_{NIR} and R_{red} represent reflectances in red and NIR bands, respectively. Here, NDVI is calculated through the use of MODIS NBAR (Nadir BRDF-Adjusted Reflectance), thus mainly representing a spectral variable that may not contain information content regarding bidirectional reflectance. As shown from Table 7, MODIS BRDF shape indicators are not well related to NDVI, implying that MODIS BRDF shape indicators have different information relative to NDVI.

Gao, *et al*. (2003) has explored the relationship between SSI and NDVI in detail. Here, we will adopt a similar approach to analyze the relationship between AFX and NDVI. However, an emphasis will be laid on the different information content contained in AFX relative to the NDVI, and on the ability of the AFX to indicate land surface anisotropic reflectance with two basic scattering types shifting. Some similar analysis can also be made of other BRDF shape indicators.

Scatter plots between AFX and NDVI in red and NIR bands are shown in Fig. 3, AFX is not highly related to NDVI, showing that AFX contains information contents different from NDVI. Generally, the large values of AFX correspond to the large values of NDVI. It shows that the AFX is somewhat similar with the NDVI, and may be a little related to vegetation biomass. However, the variation of AFX relative to NDVI shows that the AFX is different from the NDVI, and indicates land surface properties in terms of anisotropic reflectance patterns. For examples, at middle range (0.3—0.7) of NDVI values, AFX values are close to unity, while at low range (0—0.3) and high range (0.7—1.0) of NDVI values, the corresponding AFX values have wider range. Specifically, in NIR band, at lower NDVI range (0—0.3), the AFX values of wheat (CUW) are greater than soil type (S2, S3, S4 and S5) and sparse grass (GS and GA). At higher NDVI range (0.7—1.0), the AFX values of soybean (CS1 and CS2) and wheat (CIW) are greater than forest types (OBS, OJP and ASP), since crops are usually less clumped than forest and soil in structure. Such a structural difference determines that the volumetric scattering effects of crops are more prominent in NIR band. In red band, for crops especially the soybeans, the row structure make the surface scattering more prominent. As a result, Fig. 3 shows that the AFX can capture the 3D structural features, which is not available in NDVI.

The three subplots in Fig. 3 show the BRDF curves in principal plane for three typical types: rough soil (S4), flat alkali (S1) and dense wheat (CIW). As can be seen from these three subplots, the rough soil type presents a dome-shaped BRDF curve with a prominent peak reflectance at retro-solar direction. Here, we have AFX < 1. The flat alkali (S1) presents a relatively flat BRDF curve with AFX≈1, which approximately indicates a Lambertian surface. The dense wheat type presents a bowl-shaped BRDF curve with AFX > 1, which means that volumetric scattering type is dominant. Here, the radiative transfer theory may be more suitable for the description of this vegetation type. The analysis above shows that the AFX captures the BRDF shapes well in terms of its value around unity and is related to the land surface structure. From the Eq. (2), we can see that the AFX is calculated by combining the two basic scattering types: volumetric and surface scatterings that are normalized by isotropic scattering, therefore, it can provide the overall description of bidirectional reflectance. Other reflectance-based BRDF shape

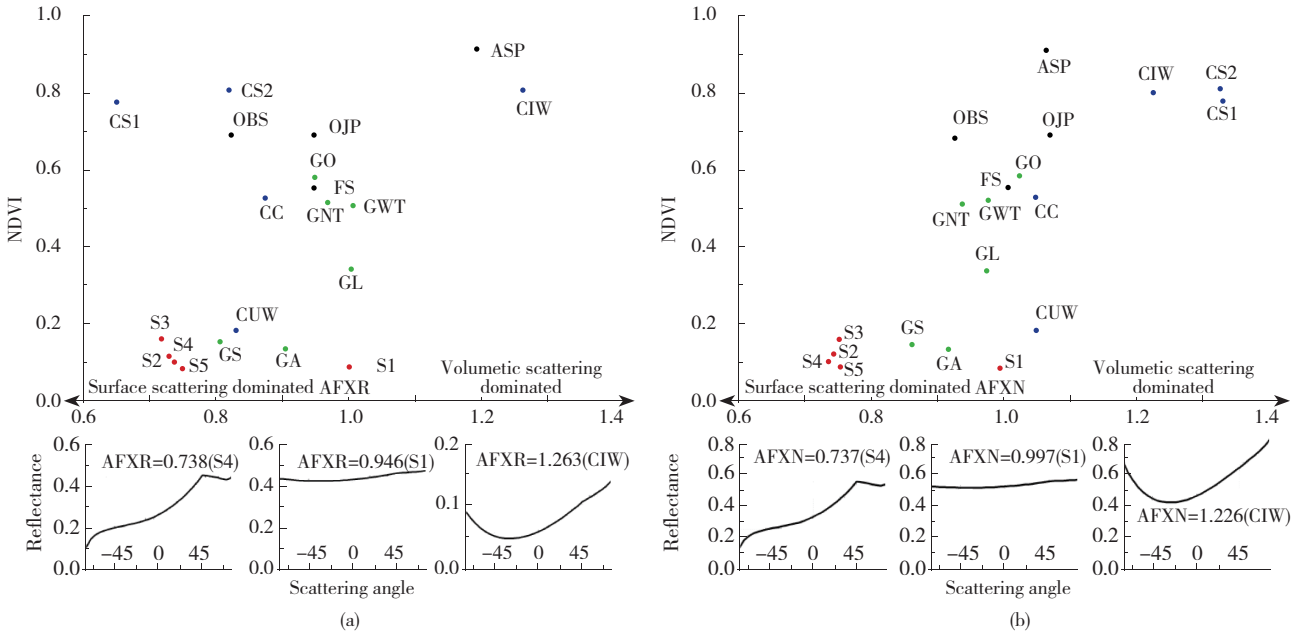

Fig. 3 (a) scatter plots between AFXR and NDVI in red band; (b) scatter plots between AFXN and NDVI in NIR band for 20 ground BRDF datasets (The three small subplots below each scatter plot represent BRDF curves for three typical types: the rough soil (S4), flat alkali (s1) and dense wheat (CIW). The positive axis of abscissa of the subplots represents backward scattering, and the negative axis of abscissa represents the forward scattering. Solar zenith angle is at 45° backward)

indicators, such as ANIX, are constructed through the use of the reflectance in two typical scattering angles, and rather than considering the overall BRDF shapes. In addition, the AFX determines the BRDF shape in terms of the relative strength between volumetric and geometric-optical effects. Thus it is considered to have some physical meanings.

4.5 Spectral effect of MODIS BRDF shape indicators

We further analyzed the spectral BRDF effects in terms of the different behaviors of BRDF shape indicators in red and NIR bands.

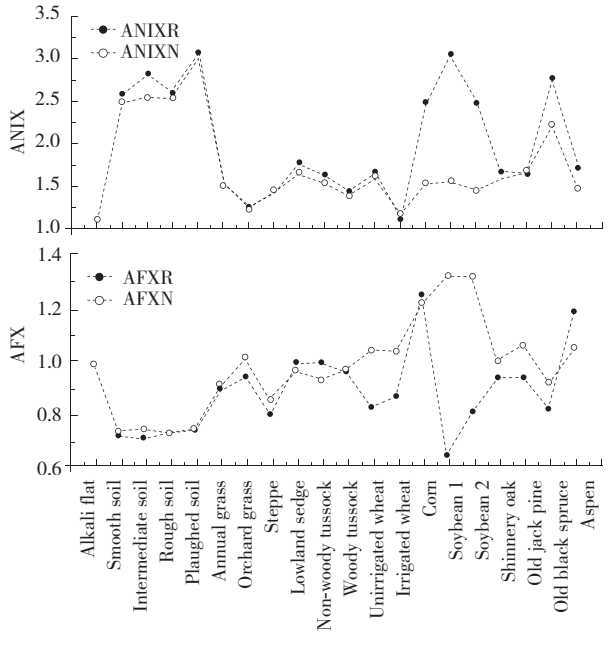

Fig. 4 the ANIX and AFX for 20 ground datasets in red and NIR bands

Kimes (1983) and Sandmeier, *et al.* (1998) have performed a detailed analysis of the hyper-spectral BRDF effects, and conclude that hyper-spectral BRDF effects are mainly caused by land surface structure, scattering properties of surface components and their interactions. Here, our major analysis focuses on the relative strength of two basic scattering types: volumetric scattering and geometric-optical scattering. As can be seen from Fig. 4, ANIX values in red band are greater than that in NIR band, especially for vegetation. Contrarily, AFX values in NIR band are greater than that in red band, also especially for vegetation since the vegetation canopy present very different scattering in red and NIR band as compared to the soil surface. As a consequence, the spectral effect of MODIS BRDF shape indicators is also related to scattering magnitude of basic scattering types.

Specially, in red band, high chlorophyll absorption of vegetation strengthens single scattering, which in turn strengthens the geometric-optical effects, while in NIR band, high leaf transmission strengthens the multiple scattering, which increases the volumetric effects. As can be seen from the kernel shapes of volumetric and geometric-optical scatterings (Fig. 1), if the geometric-optical scattering is dominant, the normalized reflectance difference between hotspot and dark spot would increase, while if the volumetric scattering is dominant, the normalized reflectance difference between hot spot and dark spot would decrease. As a result, for ANIX that is defined as reflectance ratio of hotspot to dark spot, its value in red band is often greater than that in NIR band since there are more geometric-optical scattering in red band than in NIR band. For AFX that describe the relative strength between volumetric and geometric-optical scatterings, we usually have AFX < 1 if the geometric-optical scattering is dominant and AFX > 1 if the volumetric scattering is dominant. As a result, the spectral effect of BRDF shape indicators between red and NIR bands is actually caused by the

relative strength between basic scattering types.

5 ANALYSIS WITH SATELLITE SAMPLES FROM MODIS

As mentioned above, some MODIS BRDF shape indicators such as ANIF, ANIX and NDAX were originally used to explore the physical mechanism of hyper-spectral BRDF effects, and were found to be related to vegetation structure. However, for the MODIS sensor, these shape indicators can be constructed based on the operational MODIS BRDF/Albedo algorithm since sparse sampling ability of MODIS makes it difficult to directly acquire the observations in typical scattering angle (Barnsley, *et al*., 1994). Therefore, it is necessary to further examine these shape indicators with MODIS samples. AFX and SSI are parameter-based MODIS BRDF shape indicators. SSI has been well explored with ground measurements and satellite observations from MODIS and MISR (Gao, *et al*., 2003). However, AFX still need further exploration. In this section, we will focus on the analysis of the BRDF shape indicators with MODIS observations.

5.1 Correlation analysis and principal component analysis

Correlation analysis and PCA (Principal Component Analysis) were performed with selected MODIS samples (Table 2). Due to cloud contamination, only four dates (DOY of 177, 193, 257 and 273) were selected from the study region, and R^2 was calculated in Table 8. As can be seen from Table 8, ANIF is still highly related to ANIX for MODIS samples with R^2 approximating to 0.9. This shows that a refine on MODIS BRDF shape indicators is need by removing ANIF from MODIS BRDF shape indicator products. This analysis result is basically consistent with ground measurements.

Table 8 Coefficients of determination (R^2) of MODIS BRDF shape indicators with MODIS samples

	ANIFR	ANIFN	ANIXR	ANIXN	AFXR	AFXN	NDAX	SSI
ANIFR	1.000	—	—	—	—	—	—	—
ANIFN	0.134	1.000	—	—	—	—	—	—
ANIXR	0.933	0.149	1.000	—	—	—	—	—
ANIXN	0.158	0.867	0.192	1.000	—	—	—	—
AFXR	0.535	0.050	0.314	0.039	1.000	—	—	—
AFXN	0.059	0.711	0.057	0.399	0.043	1.000	—	—
NDAX	0.587	0.031	0.604	0.023	0.279	0.027	1.000	—
SSI	0.112	0.153	0.064	0.050	0.280	0.303	0.030	1.000

The PCA was then performed on the MODIS samples to explore the intrinsic dimension of the MODIS BRDF shape indicators. PCA technique transforms original datasets into orthogonal datasets named as PCs (Principal Component) through the use of a linear transformation technique. Therefore, there are no correlations between PCs. With the PCA technique, we can analyze the relationships between PCs and the physical meanings that the first few PCs represent. Here, we perform a principal component transformation on four dates of MODIS sample pixels for MODIS BRDF shape indicators to obtain eigenvalues and explained variance percentage of each PC (Table 9). Since MODIS BRDF shape indicators are constructed in different ways and have different meanings, correlation matrix was used to calculate the PCs.

As can be seen from Table 9, the total variance percentage for the first three PCs are greater than 90%, indicating that MODIS BRDF shape indicators are approximately intrinsic three-dimensional. Table 10 describes the weight coefficients for each PC of MODIS BRDF shape indicators. Since the first three PCs can explain most variances of these indicators, potential meanings for the first three PCs are mainly explored in this study.

Table 9 Eigenvalues and explained variance percentage for each PC of MODIS BRDF shape indicators

PC	eigenvalue	Var. Perc./%
1	3.9533	49.4161
2	2.3517	29.3957
3	0.9937	12.4218
4	0.4051	5.0638
5	0.2165	2.7058
6	0.0601	0.7517
7	0.0150	0.1879
8	0.0046	0.0572

Table 10 Weighting coefficients for different PCs of MODIS BRDF shape indicators

PCs	ANIFR	ANIFN	ANIXR	ANIXN	AFXR	AFXN	NDAX	SSI
PC1	–0.444	–0.357	–0.4273	–0.336	0.361	0.311	–0.254	0.297
PC2	0.273	–0.440	0.2523	–0.382	–0.229	0.426	0.529	0.092
PC3	–0.165	–0.164	–0.3121	–0.374	–0.350	–0.182	–0.049	–0.742
PC4	0.036	0.024	–0.2265	0.267	–0.732	0.394	–0.370	0.220
PC5	–0.039	0.001	0.1129	0.398	0.316	0.653	–0.040	–0.547
PC6	–0.521	0.242	–0.3096	0.253	–0.138	0.039	0.696	0.075
PC7	0.134	0.767	–0.0778	–0.531	0.045	0.323	–0.018	0.002
PC8	–0.640	0.067	0.7003	–0.159	–0.197	0.031	–0.174	0.010

As can be seen from the first eigenvector, all weight coefficients of BRDF shape indicators in the first eigenvector seem to be close. Weight coefficients for the red band are somewhat larger than for NIR band for the first PC, showing that the red band contributes more on the first PC than the NIR band does. From the sigh of weights of the first PC, we can see that the MODIS BRDF shape indicators are divided into two groups: reflectance-based BRDF shape indicators and parameter-based BRDF shape indicators. These two groups are negatively correlated. The reflectance-based BRDF shape indicators including ANIF, ANIX and NDAX show negative coefficients in the first PC. The parameter-based BRDF shape indicators including AFX and SSI present positive coefficients in the first PC. The negative correlations between these two groups can be well explained from their formulas (Table 1).

Specifically, from their formulas, we can infer that SSI and AFX increase with volumetric effects growing. From the analysis of ba-

sic scattering types that constitute the operational MODIS BRDF/Albedo algorithm, we can see that volume-dominated scattering type presents a bowl-shaped BRDF curve, while geometric-optics-dominated scattering type presents a dome-shaped BRDF curve with a strong hot spot in retro-solar direction. With the geometric-optical scattering transiting to volumetric scattering, the contrast between hotspot and dark spot tends to decrease. Therefore, ANIX, the ratio of hotspot to dark spot tends to decrease. As ANIF and ANIX are highly correlated, so ANIF also tends to decrease, as well as NDAX that is constructed by normalizing red and NIR ANIX. The above analysis shows that, with basic scattering types changing from geometric-optical scattering to volumetric scattering, reflectance-based MODIS BRDF shape indicators show negative correlation with parameter-based BRDF shape indicators. This is the physical meaning that the first PC captures.

Investigation of weight coefficients of the second eigenvector shows that the weights in NIR band are greater than in red band, and that weights in red and NIR bands also present negative correlations, indicating that the second PC mainly represents spectral difference for ANIF, ANIX and AFX in red and NIR bands. Differing from the spectral effect of nadir reflectance in red and NIR bands, the spectral effect of these three shape indicators mainly reflects the spectral difference of anisotropic reflectance patterns in red and NIR bands. As for MODIS anisotropic scattering pattern, geometric-optical effect is usually greater than volumetric effect in red band, and vice versa in NIR band, which generates a dome-shaped BRDF curve in red and a bowl-shaped BRDF curve in NIR. As can be seen from the analysis above, vegetation canopy usually presents different anisotropic reflectance pattern in red and NIR bands due to different surface structure and scattering types. This is the physical meaning captured by the second PC.

As for the third PC, SSI has maximum weight coefficient, and all coefficients are negative in sign, indicating that all MODIS BRDF shape indicators have similar interpretations in third PC. As all MODIS BRDF shape indicators are constructed through the use of anisotropic scattering pattern which is, in turn, related to land surface structures, so the third PC may be mainly related to structural characteristics of land surface. Investigation of Table 9 shows that the third PC accounts for about 12% total variance percentage, indicating that the third PC could provide secondary information content in identifying land cover types. If the third PC is majorly related to land surface structure, this shows that the MODIS BRDF shape indicators do provide additional information content regarding land surface structure although the information content contained in this PC is somewhat marginal as compared with spectral signatures.

5.2 Analysis of within-class variance of MODIS BRDF shape indicators

With the selected MODIS sampling datasets, we calculate the within-class variances for several typical land surface types in the study region. It is important to apply these BRDF shape indicators to improve classification accuracy. Sandmeier, *et al*. (1999) and Bicheron, *et al*. (2000) realized that the ANIX has great within-class variances. This study uses selected MODIS samples to calculate mean, variance and coefficient of variation for ANIX and AFX, and analyze the variance variation for these shape indicators in red and NIR bands. Coefficient of variation is defined as the ratio of standard deviation to mean, and it removes the between-variable difference caused by their different units and average.

Fig.5 presents mean, variance and coefficient of variation for ANIX and AFX in red and NIR bands. Inspection of Fig. 5 shows that the mean of ANIX and AFX are negatively correlated in red and NIR bands. ANIX values in red band are greater than in NIR band, and vice versa for AFX. This is obviously consistent with the analysis on the 1st PC in PCA. As mentioned above, the physical mechanism of the BRDF spectral effect is attributed to relative strength between geometric-optical and volumetric effects, and is related to the structure of land surface.

A further analysis of the mean tendency (Fig. 5) is performed in terms of class characteristics for each of seven selected IGBP classes. The vegetation types used in this study are generally divided into two groups: forest type with discrete vegetation structure and herbaceous type with continuous vegetation structure. For the former, the evergreen needleleaf forest has a typical clumping structure for different hierarchic rank: from needles to clusters, to branches, to crown, to forest, and finally to landscape scale. The non-randomly distributed hierarchical structure of the evergreen needleleaf forest determines that the shadow effects may be dominant within this class. Conversely, for the herbaceous type such as grassland and cropland, their structures are usually assumed to be randomly distributed. Therefore, radiative transfer theory may suitably describe such structures. As we know, reciprocal LiSparse kernel provides a dome-shaped BRDF curve, while the RossThick kernel provides a bowl-shaped BRDF curve. The true BRDF shapes are actually weighted by these two curves. They are band-dependent due to the absorption and scattering of surface components to solar radiation, and are therefore related to geometric-optical and volumetric effects.

Investigation of the variance change of different vegetation types in red and NIR bands in Fig. 5 shows that the variances in red band seem to be higher than that in NIR band. The coefficient of variation in Fig. 5 obviously presents such a trend as well. A comparison of the coefficient of variation between ANIX and AFX shows that AFX has lower within-class variances than ANIX does, showing that AFX may be more useful in differentiating land cover types.

In order to investigate phenology of vegetation types changing with geometric-optical scattering and volumetric scattering, we calculate mean of phenological dates for MODIS samples for each of land cover types in study region (Table 11). As can be seen from Table 11, the phenological dates for each of seven land cover types in the study region are not prominently different, generally onset of greenness in mid-May, onset of greenness maximum in late June to mid-July, onset of greenness decrease in late August, and onset of greenness minimum by the end of September to early October.

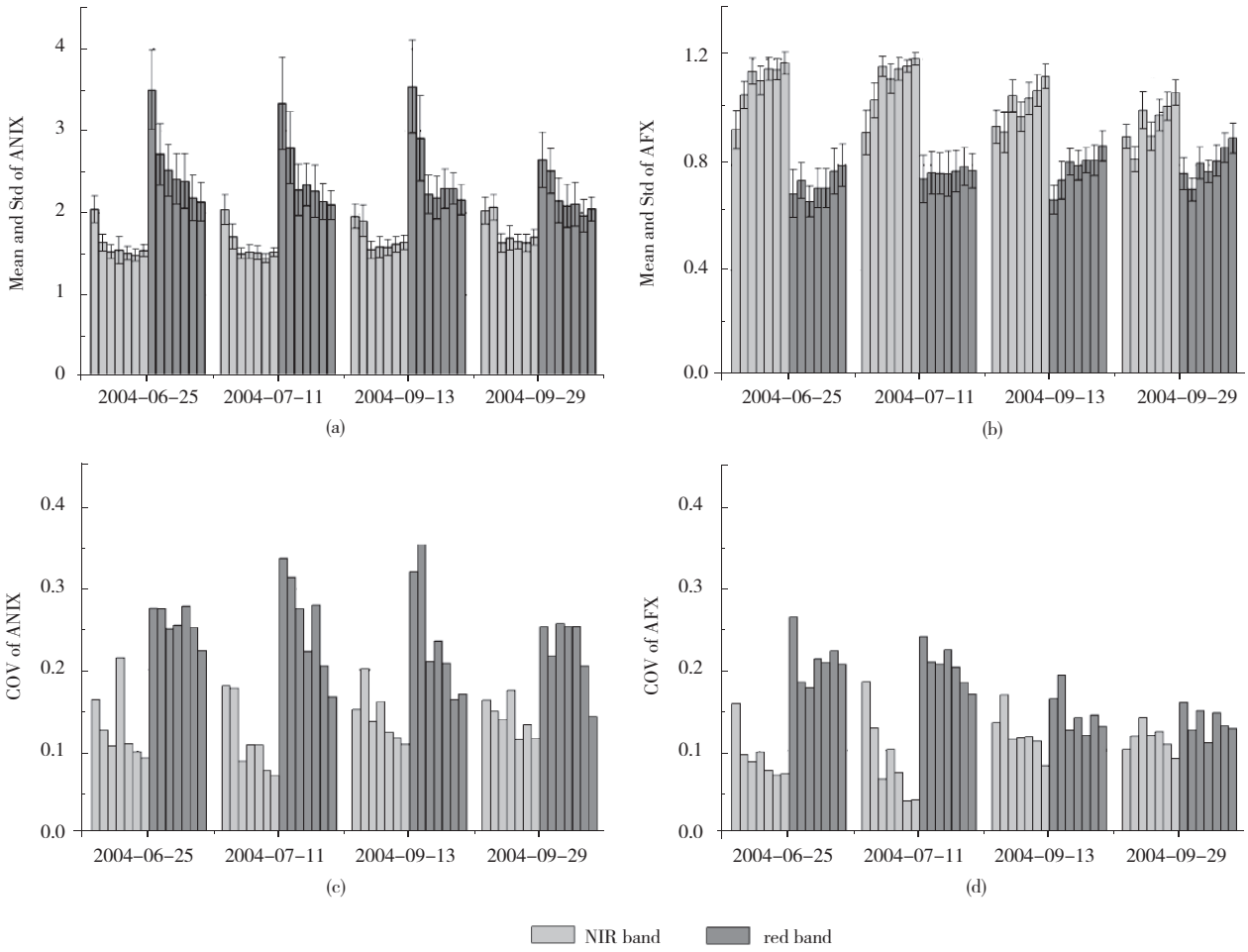

Fig. 5 Mean, variance and coefficient of variation (CoV) of ANIX (a and c) and AFX (b and d) in red and NIR bands (Abscissa represent different dates. White gray clusters represent red bands, and gray clusters represent NIR band. Each of seven bars respectively represents the evergreen needleleaf forest (ENF), mixed forest (MF), open shrubland (OS), woody savanna (WS), grassland (GL), cropland (CL), and cropland and natural vegetation mosaic (CLVM). The error bars in subplot (a) and (b) represent one standard deviation. Solid line crossed the subplot (b) represent AFX=1, indicating that the anisotropy reflectance of the selected IGBP types approaches to Lambertian at AFX=1)

Table 11 Phenological dates for MODIS samples

	OGI	OGmax	OGD	OGmin
ENF	05–18	07–08	08–23	09–26
MF	05–17	06–27	08–25	10–03
OS	05–22	07–12	08–30	10–04
WS	05–20	07–03	08–26	10–03
GL	05–20	07–10	08–28	10–05
CL	05–20	07–17	08–23	10–05
CNVM	05–11	07–15	08–18	10–08

OGI, OGmax, OGD, OGmin represent Onset of Greenness Increase, Onset of Greenness Maximum, Onset of Greenness Decrease and Onset of Greenness Minimum, Units(month/day). ENF, MF, OS, WS, GL, CL and CNVM are same as in Fig.7.

As can be known from the previous analysis, the relative strength between geometric-optical and volumetric scatterings determines that AFX varies around unity. From Fig. 5, we can also see that an AFX < 1 in red band for all IGBP land cover types for 4 phenological dates implies the geometric-optical scattering is dominant, thus indicating a dome-shaped BRDF curve. However, the geometric-optical scattering and volumetric scattering are alternately dominant in NIR band for all selected land cover types with phenological dates progressing. Specifically, evergreen needleleaf forest type bears more geometric-optical effect than volumetric effect, thus an AFX < 1 is expected; vice versa for Cropland and Cropland and natural vegetation mosaic with an AFX > 1. For other vegetation types including Mixed forests, Open shrubland, Woody savanna and Grassland, in the growing season, an AFX > 1 indicates that volumetric scattering effect is greater than geometric-optical scattering effect, while in dormant season, with vegetation leaves withering, the volumetric scattering decreases and the surface scattering increases, thus an AFX > 1 indicates that the geometric-optical scattering is greater than the volumetric scattering. From point of view of vegetation structure, the evergreen needleleaf forest type is hierarchically clumped, while the Cropland canopy is usually assumed to be randomly distributed in structure.

The mixed forest type is between them with structure changing with different seasons. Therefore, we can distinguish different land cove types, and explore vegetation seasonal change with MODIS BRDF shape indicators.

6 CONCLUSIONS AND DISCUSSION

MODIS BRDF shape indicators are constructed from the anisotropic reflectance patterns through the use of the semi-empirical kernel-driven BRDF model. This study performs a comprehensive analysis of MODIS BRDF shape indicators with a variety of ground measurements and satellite samples from MODIS. The study shows that MODIS BRDF shape indicators are different from spectral vegetation index such as NDVI, containing the information content regarding vegetation structure. Therefore, MODIS BRDF shape indicators may be used to extract the structural information of land surface. The correlation analysis with ground measurements and selected MODIS samples shows that the ANIF is highly related to ANIX in red and NIR bands. As the ANIX is defined as the ratio of hotspot to dark spot, and has an advantage of wide value range over ANIF. Therefore, we suggest refine MODIS BRDF shape indicators by removing the ANIF from MODIS BRDF shape indictor products.

The principal component analysis shows that the MODIS BRDF shape indicators are intrinsically three dimensional. The meanings for the first three PCs are well explained. The first PC explains the way in which MODIS BRDF shape indicators are constructed. The second PC explains the spectral effect of MODIS BRDF shape indicators. As the third PC comes from same type of contributions and accounts for about 10% of total variance percentage, it may be mainly related to the structural characteristics of land surface.

We further investigate the relationship between BRDF shapes and AFX, and find that AFX is related to the relative strength between volumetric and geometric-optical scatterings. AFX indicates BRDF shape in terms of its value around unity. An AFX < 1 shows a surface scattering dominant, indicating a dome-shaped BRDF curve with a prominent reflectance peak (hotspot) in retro-solar direction. An AFX > 1 presents a volumetric scattering dominant, indicating a bowl-shaped BRDF curve where reflectance near nadir is lower than for larger scattering angles with the minimum usually displaced towards the forward scattering direction in principal plane. AFX≈1 indicates a relatively flat BRDF curve. AFX changes with band and phenological date, and is related to land cover type and the land surface structure.

Within-class variances of MODIS BRDF shape indicators are usually larger in red than in NIR band. For same type, the within-class variances for AFX are usually less than for ANIX. Therefore, AFX may be more useful than ANIX in improving classification accuracy as additional signatures of nadir spectral reflectance.

MODIS BRDF shape indicators are now among the operational MODIS BRDF/Albedo products. With the operational MODIS BRDF/Albedo products updated and the new planed environmental satellite system such as NPOESS (National Polar-orbiting Operational Environmental Satellite System) into operation, the findings of this study will play important and practical roles on how to construct and expand the application of BRDF shape indicators.

MODIS BRDF shape indicators are only valid for the full inversion of MODIS BRDF/Albedo products. However, it is difficult to acquire the full-inversion MODIS BRDF shape indicators for a whole region and a continuous date due to the contamination of clouds and aerosols, although the Terra and Aqua are currently combined into the operational MODIS BRDF/Albedo products. This brings much difficulty for further application of MODIS BRDF shape indicators to a larger region and long time series. One solution is to use time series of MODIS BRDF products to fill gaps and generate a high-quality product. This is a potential research direction in future study.

Acknowledgements: Thanks are due to a number of colleagues for their help, advice, and encouragement in relation to various aspects of this paper, in particular, Crystal Schaaf (Geography and Environment Department, Boston University, USA).

REFERENCES

Barnsley M J, Strahler A H, Morris K P and Muller J P. 1994. Sampling the surface bidirectional reflectance distribution function (BRDF): evaluation of current and future satellite sensors. *Remote Sensing Review*, **8**: 271–311

Bicheron P and Leroy M.2000. Bidirectional reflectance distribution function signatures of major biomes observed from space. *Journal of Geophysical Research*, **105** (D21): 26669–26681

Deering D W, Eck T F and Banerjee B. 1999. Characterization of the reflectance snisotropy of there boreal forest canopies in spring-summer. *Remote Sensing of Environment*, **67**: 205–229

Deering D W, Eck T F and Grier T. 1992. Shinnery oak bidirectional reflectance properties and canopy model inversion. *IEEE Transactions on Geoscience and Remote Sensing*, **30** (2): 339–348

Deering D W, Eck T F and Otterman J. 1990. Bidirectional reflectances of three desert surfaces and their characterization through model inversion. *Journal of Agricultural and Forest Meteorology*, **52**: 71–93

Defries R S, Hansen M C, Townshend J R G, Janetos A C and Loveland T R. 2000. A new global 1-km dataset of percentage tree cover derived from remote sensing. *Global Change Biology*, **6**: 247–252

Friedl M A, McIver D K, Hodges J C F, Zhang X Y, Muchoney D, Strahler A H, Woodcock C E, Gopal S, Schneider A, Cooper A, Baccini A, Gao F and Schaaf C. 2002. Global land cover mapping from MODIS: algorithms and early results. *Remote Sensing of Environment*, **83**: 287–302

Gao F, Schaaf C B, Strahler A H, Jin Y and Li X. 2003. Detecting vegetation structure using a kernel-based BRDF Model. *Remote Sensing of Environment*, **86**: 198–205

Hu B, Lucht W, Li X and Strahler A H. 1997. Validation of kernel-driven semiempirical models for the surface bidirectional reflectance distribution function of land surfaces. *Remote Sensing of Environment*, **62**: 201–214

Irons J R, Campbell G S, Normal J M, Graham D W and Kovalick W M. 1992. Prediction and measurement of soil bidirectional reflectance. *IEEE Transactions on Geoscience and Remote Sensing*, **30** (2): 249–260

Jin Y, Schaaf C B, Gao F, Li X, Strahler A H, Lucht W and Liang S. 2003. Consistency of MODIS surface bidirectional reflectance distribution function and albedo retrieval: Algorithm Performance. *Journal of Geophysical Research*. DOI: 10.1029/ 2002JD002803

Kimes D S. 1983. Dynamics of directional reflectance factor distributions for vegetation canopies. *Applied Optics*, **22**(9): 1364–1372

Kimes D S, Newcomb W W and Tucker C J. 1985 Directional reflectance factor distributions for cover types of Northern Africa. *Remote Sensing of Environment*, **18**: 1–19

Lucht W, Schaaf C B and Strahler A H., 2000. An Algorithm for the retrieval of Albedo from space using semiempirical BRDF Models. *IEEE Transactions on Geoscience and Remote Sensing*, **38** (2): 977–998

Nicodemus F E, Richmond J C, Hsia J J, Ginsberg W I and Limperis T. 1977. Geometrical Considerations and Nomenclature for Reflectance. Washington, D.C.: Institute for Basic Standards

Ranson K J, Biehl L L. and Bauer M E. 1985. Variation in spectral response of soybeans with illumination, view, and canopy geometry. *International Journal of Remote Sensing*, **6** (12): 1827–1842

Roujean J L, Leroy M and Deschamps P Y. 1992. A bidirectional reflectance model of the earth's surface for the correction of remote sensing data. *Journal of Geophysical Research*, **97**: 20455–20468

Roujean J L, Tanre D, Breon F M and Deuze J L.1997. Retrieval of land surface parameters from airborne POLDER bidirectional reflectance distribution function during HAPEX-Sahel. *Journal of Geophysical Research*, **102** (D10): 11201–11218

Sandmeier S R and Deering D W. 1999. Structure analysis and classification of boreal forest using airborne hyperspectral BRDF data from ASAS. *Remote Sensing of Environment*, **69**: 281–295

Sandmeier S R, Muller C, Hosgood B and Andreoli G. 1998. Physical mechanisms in hyperspectral BRDF data of grass and watercress. *Remote Sensing of Environment*, **66**: 222–233

Schaaf C B, Gao F, Strahler A H, Lucht W, Li X, Tsang T, Strugnell N C, Zhang X, Jin Y, Muller J P, Lewis P, Barnsley M, Hobson P, Disney M, Roberts G, Dunderdale M, Doll C, Entrmont R P, Hu B, Liang S, Privette J L and Roy D. 2002. First operational BRDF/ Albedo nadir reflectance products from MODIS. *Remote Sensing of Environment*, **83**: 135–148

Shuai Y, Schaaf C B, Strahler A H, Liu J and Jiao Z. 2008. Quality assessment of BRDF/albedo retrievals in MODIS operational system. *Journal of Geophysical Research*. DOI:10.1029/2007GL032568

Vierling L A, Deering D W and Eck T F. 1997. Differences in arctic tundra vegetation type and phenology as seen using bidirectional radiometry in the early growing season. *Remote Sensing of Environment*, **60**: 71–82

Wanner W, Li X and Strahler A H. 1995. On the derivation of kernels for kernel-driven models of bidirectional reflectance. *Journal of Geophysical Research*, **100**: 21077–21090

Zhang X, Friedl M A, Schaaf C B, Strahler A H, Hodges J C, Gao F, Reed B C and Huete A. 2003. Monitoring vegetation phenology using MODIS. *Remote Sensing of Environment*, **84**: 471–475

评估MODIS的BRDF角度指数产品

焦子锑，李小文，王锦地，张虎

遥感科学国家重点实验室 北京师范大学；北京师范大学 地理学与遥感科学学院；
北京环境遥感与数字城市北京市重点实验室，北京 100875

摘 要：应用地表观测的二向性反射数据集和多种MODIS数据产品，通过统计分析，对MODIS的二向性反射角度指数产品进行综合评估，结果表明：(1)MODIS角度指数包含了地表三维结构信息，有望用来反演地表的物理结构参数；(2)MODIS角度指数是内在的三维关系，各向异性因子(Anisotropic Factor: ANIF)和各向异性指数(Anisotropic Index: ANIX)高相关，建议去掉ANIF以精炼MODIS角度指数产品；(3)各向异性平整指数(Anisotropic Flat Index: AFX)较好地指示了地表基本散射类型的变化，且具有较小的类内方差，对改善特定地表分类精度可能会更有用。

关键词：MODIS，BRDF，角度指数，植被结构，植被指数

中图分类号：TP701 **文献标志码**：A

引用格式：焦子锑，李小文，王锦地，张虎. 2011. 评估MODIS的BRDF角度指数产品. 遥感学报，**15**(3): 432–456
Jiao Z T, Li X W, Wang J D and Zhang H. 2011. Assessment of MODIS BRDF shape indicators. *Journal of Remote Sensing*, **15**(3): 432–456

1 引 言

多年来，大量的地表观测和建模研究工作已表明地表反射表现为各向异性，它通常由二向性反射分布函数(BRDF)来描述。二向性反射分布函数定义了给定波段的表面散射作为照明和观测几何的函数(Nicodemus 等，1977)。BRDF模型建立了二向性反射与地面目标的光谱属性和结构特征的关系，因此，如果给定地面目标的光谱和结构参数，BRDF模型可以提供前向模拟，得到地表各向异性反射模式。反之，如果给定地表各向异性的反射模式，通过BRDF模型也可能进行后向反演，以推断植被结构等地表参数。

根据地表的各向异性反射模式来推断植被结构通常可归纳为3种方式(Gao 等，2003)：一是根据模型反演的基本原理和方法，直接用物理的BRDF模型来反演地表参数，如植被结构等。但由于物理模型复杂和不易操作，因此，几个在轨运行的多角度卫星传感器如POLDER，MODIS和MISR等都通过应用半经验的BRDF模型，作为计算地表反照率的主算法。半经验和核驱动的BRDF模型采用了几个经验函数(所谓的核)加权和的形式来拟合地表的BRDF形状，这些核的推导基于一些近似的物理假设，因而有物理含义。反演这些核驱动模型得到的是核的权重系数，并不是直接得到地表结构参数。然而这些权重系数的表达式包含了地表结构参数的信息(Roujean 等，1992；Wanner 等，1995)，因此，提供了一种反演地表结构参数的可能性，这为利用地表各向异性反射模式来推断地表结构参数提供了第二种方式(Roujean 等，1997；Gao 等，2003)。

第三种方式通常是应用各向异性的反射模式在典型散射角(如热点、冷点和天顶)的反射率，构造二向性反射角度指数，以研究地表结构与这些角度指数的关系。Sandmeier 等(1998，1999)通过利用典型

收稿日期：2010-03-05；**修订日期**：2010-09-30

基金项目：国家自然科学基金(编号：40871193)；遥感科学国家重点实验室自由探索项目(编号：10ZY-06)；国家重点基础研究发展计划(973计划)(编号：2007CB714402-8)。

第一作者简介：焦子锑(1970—)，男，副教授，2009年毕业于波士顿大学地理与环境系，获博士学位，现从事定量遥感、地表各向异性反射的建模与应用，多角度信号对地表分类贡献的研究，已发表论文20余篇。E-mail: jiaozt@bnu.edu.cn。

散射角在热点、天顶和冷点的反射，构造了各向异性因子(ANIF)、各向异性指数(ANIX)和归一化的各向异性指数(Normalized Difference Anisotropy Index: NDAX)。基于两种典型结构的植被类型(喜平型和喜直型)，分析了二向性反射光谱效应的物理机制，认为这些二向性反射角度指数和地表结构有关，并以加拿大北方林为实验区，将这些角度指数应用于地表分类实验中，研究了这些角度指数对提高地表分类精度的作用。结果表明，这些二向性反射角度指数可以改善某种地表类型的分类精度。

MODIS的二向性反射角度指数(BRDF形状指示因子)产品是MODIS二向性反射产品的重要组成部分，有助于拓展BRDF遥感数据的应用。通过借用已有的二向性反射角度指数的构造方式和反演得到的BRDF模型参数，MODIS的二向性反射和反照率产品也提供了几个角度指数的产品。其中，ANIF、ANIX和各向异性平整指数(AFX)依赖于波段，即对每一波段都可以计算得到一个角度指数。但MODIS只提供它们在红和近红外波段的值，用户可以根据需要，方便地计算它们在MODIS其他波段的值。NDAX是ANIX在红和近红外波段进行归一化处理的结果。结构散射指数(Structural Scattering Index: SSI)是利用MODIS近红外波段的体散射参数和红波段的几何光学参数，经验构造而成(Gao 等，2003)。在MODIS的角度指数产品中，SSI用地面测量的BRDF数据系及星载的MODIS和MISR采样数据进行过全面验证，结果表明，SSI可用来探测植被结构的变化或区分不同的地表类型。AFX是根据核驱动模型的构造特点，针对MODIS传感器的各向异性反射模式而构造的角度指数，但对该指数的详细论述还很不够。

本文用几十组地表观测的二向性反射数据系和4种MODIS陆地表面产品，综合评价了MODIS的各向异性的角度指数产品。第2部分对MODIS二向性反射指示因子进行公式化表示，并给出了各向异性平整指数的另一种表达形式；第3部分主要描述了所用的数据；第4部分针对地表二向性观测数据对MODIS的各向异向角度指数进行了分析；第5部分应用MODIS相关的星载采样数据对MODIS的二向性反射角度指数进行了分析，最后给出结论和讨论。本文着重分析了AFX对BRDF形状的指示能力及其与植被结构的关系。

2 MODIS二向性反射角度指数的公式化

核驱动的MODIS BRDF/Albedo主算法采用了两个核的线性加权和的形式，这两个核称之为罗斯表层核(RossThick)和李氏稀疏互易核(LiSparse-Reciprocal)。核驱动的半经验模型有如下的构造形式(Roujean 等，1992；Wanner 等，1995；Lucht 等，2000)

$$R(\theta,\vartheta,\phi,\Lambda)=f_{\mathrm{iso}}(\Lambda)+f_{\mathrm{vol}}(\Lambda)K_{\mathrm{vol}}(\theta,\vartheta,\phi)+f_{\mathrm{geo}}(\Lambda)K_{\mathrm{geo}}(\theta,\vartheta,\phi) \quad (1)$$

式中，K_{geo}和K_{vol}为几何光学核和体散射核，它们分别是观测角θ和照明角ϑ及相对方位角ϕ的三角函数；f_{iso}，f_{geo}和f_{vol}是常系数，分别表示各向同性散射，几何光学散射和体散射这三部分所占的权重；$R(\theta,\vartheta,\phi,\Lambda)$是$\Lambda$波段的二向性反射分布函数。

核驱动模型通过线性回归，反演出拟合观测数据最优的f_{iso}，f_{geo}和f_{vol}，然后通过核的外推或内插可求出任意光线入射角和观察角的二向反射。计算反照率时，因为核是与待反演参数无关的函数，核的积分可预先求出，只要把核的积分以f_{iso}，f_{geo}和f_{vol}为权重相加，就得到相应的黑半球或白半球反照率。作为一种半经验模型，核驱动模型具有经验模型的简洁、高速、数据拟合能力强等优点，使之能够处理来自地球观测系统(EOS)的大量数据。同时，几何光学核与体散射核都有一定的物理意义，这使得我们在外推到没有观测数据的方向时，有希望能够解释和控制外推的结果。

MODIS二向性反射角度指数包含了5个产品，这5个角度指数的公式化表示如表1所示：

表1 MODIS二向性反射角度指数

名称	缩写	公式化表示
各向异性因子	ANIF	$\mathrm{ANIF}(\Lambda)=\frac{R_{\_\mathrm{nad}}(\Lambda)}{R_{\_45\mathrm{fw}}(\Lambda)}$
各向异性指数	ANIX	$\mathrm{ANIX}(\Lambda)=\frac{R_{\_45\mathrm{bw}}(\Lambda)}{R_{\_45\mathrm{fw}}(\Lambda)}$
归一化的各向异性角度指数	NDAX	$\mathrm{NDAX}=\frac{\mathrm{ANIXR}-\mathrm{ANIXN}}{\mathrm{ANIXR}+\mathrm{ANIXN}}$
结构散射指数	SSI	$\mathrm{SSI}=\ln\left(\frac{f_{\_\mathrm{vol}\_\mathrm{NIR}}}{f_{\_\mathrm{geo}\_\mathrm{red}}}\right)$
各向异性平整指数	AFX	$\mathrm{AFX}=\frac{\mathrm{WSA}(\Lambda)}{f_{\_\mathrm{iso}}(\Lambda)}$

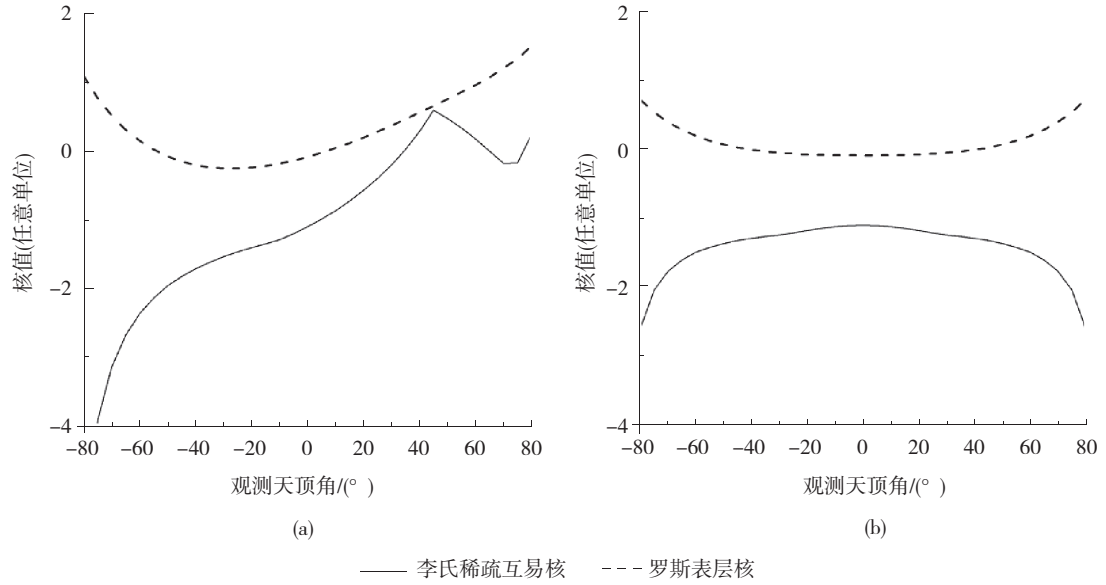

图1 主平面和垂直主平面的罗斯表层核和李氏稀疏互易核的BRDF模型核的值(罗斯表层核乘以2，太阳位于45° 太阳天顶角，李氏稀疏互易核参数h/b=2.0, b/r=1.0)
(a)主平面(PP)；(b)垂直主平面(CP)

式中，$R_{_nad}$是指天顶观测方向的反射率；$R_{_45fw}$和$R_{_45bw}$是指当太阳天顶角在45° 方向时，观测天顶角为前向45° 和后向45° 的反射率；ANIXR和ANIXN是指红和近红外波段的各向异性指数(ANIX)；$f_{_vol_NIR}$和$f_{_geo_red}$是指近红外波段的体散射参数和红波段的几何光学散射参数；$f_{_iso}$是指各向同性参数；WSA是白半球反照率，即半球-半球反照率。

我们从核驱动模型公式出发，推导了各向异性平整指数(AFX)的另一种表达形式，如式(2)：

$$\mathrm{AFX}(\Lambda)=1+\frac{f_{\mathrm{vol}}(\Lambda)}{f_{\mathrm{iso}}(\Lambda)}\times 0.189184-\frac{f_{\mathrm{geo}}(\Lambda)}{f_{\mathrm{iso}}(\Lambda)}\times 1.377622 \tag{2}$$

式中，系数0.189184和1.377622分别是对罗斯表层核和李氏稀疏互易核的双半球的积分值。

从式(2)可以看出，AFX是被各向同性参数归一化的几何光学权重参数和体散射权重参数与两个核的积分的线性表达式。AFX的大小依赖于几何光学和体散射这两个参数的大小，当体散射效应大于几何光学效应时，AFX>1；当几何光学效应大于体散射效应时，AFX<1；否则AFX≈1。由罗斯表层核和李氏稀疏互易核的形状(图1)，可以看出，李氏稀疏互易核是一个在后向散射方向上，尤其在热点方向上，表现为峰值的屋顶状；而罗斯表层核是一个典型的、略为前倾的碗状。因此，在实际观测中，根据不同地表类别的二向性反射数据，计算得到的BRDF形状，基本为这两种形状的复合。AFX<1表示几何光学散射类型主导，指示着一个屋顶状的BRDF形状；AFX>1表示体散射类型主导，指示着一个碗状的BRDF形状；否则，AFX≈1，指示一个较平的BRDF形状。我们在下面的研究中，将分别基于地表BRDF观测和MODIS的采样数据，对AFX的这一特性进行分析。

3 数据描述

3.1 地表BRDF观测数据系

本研究所用的地表BRDF观测是由多名研究者收集，这些数据系覆盖了不同的地表类型，包括不同粗糙度的裸土，不同植被覆盖度和叶面积指数的草、农作物和林地。所有这些地表类型的测量都包括几个太阳天顶角度。这些地表观测数据的总结如表2所示。我们首先用核驱动的BRDF模型拟合这些地表观测，得到该模型的3个参数，然后根据模型的3个参数计算出各向异性角度指数。本研究所用的大部分BRDF观测数据，曾被用来验证半经验的核驱动模型的拟合能力(Hu 等，1997)。

3.2 相关的MODIS星载产品

本研究我们使用了4个MODIS陆地表面产品，包括MODIS BRDF/Albedo产品(Schaaf 等，2002)，MODIS地表分类产品(Friedl 等，2003)，MODIS的植

表2 地表BRDF数据系物理特征描述

编码	分类	地表类型	太阳天顶角/(°)	覆盖度/%	叶面积指数	粗糙度/高度/cm	描述	数据源
S1		平坦盐碱地	NA	0	0	NA	亮白色	(Deering 等，1990)
S2		细粒土壤	36—53	0	0	1.2 ± 0.2	土壤湿度5.5%; 反照率19.725%	(Irons，1992)
S3	土壤	中粒土壤	16—52	0	0	2.6 ± 0.4	土壤湿度4.9%;反照率17.23%	(Irons，1992)
S4		粗粒土壤	28—54	0	0	3.9 ± 0.7	土壤湿度4.25%;反照率21.375%	(Irons，1992)
S5		犁耕裸地	26, 30, 45	0	0	8.0(深)		(Kimes，1985)
GA		年生草地	28—50	< 5	NA	<3		(Kimes，1985)
GO		果园草地	45—82	50	1.1	NA		(Kimes，1983)
GS		干枯草原	27—63	18(20% 绿)	NA	38	单丛覆盖度约为70%	(Kimes，1985)
GL	草地	低洼莎草	53—69	NA	约为0	NA	凋谢的植被	(Vierling，1995)
GNT		非木质草丛	47—75	NA	NA	NA	枯叶和绿叶混合的植被	(Vierling，1995)
GWT		木质草丛	49—75	NA	NA	NA	枯叶、绿叶和嫩叶混合的灌木丛	(Vierling，1995)
CUW		没灌溉小麦	27—51	14(95% 绿)	NA	46		(Kimes，1985)
CIW		灌溉小麦	26—59	70	NA	76	15 d内收割	(Kimes，1985)
CC	农作物	玉米地	23—68	25	0.65	33	玉米幼苗、梨耕的土壤	(Kimes，1983)
CS1		大豆地1	20—49	72	3.0	NA	行播大豆(没封垄)	(Ranson，1985)
CS2		大豆地2	21—38	83	3.9	NA	行播大豆(没封垄)	(Ranson，1985)
FS		矮丛栎	31—71	60.2	1.75	43	开放低矮的林地，黑色霉质枯叶下垫面	(Deering，1992)
OJP	林地	短叶松	35—73	61*	2.2—2.6	NA	下垫面为亮色鹿苔	(Deering，1999)
OBS		黑云杉	35—70	55	3.7—4.0	NA	下垫面为黑云杉幼苗	(Deering，1999)
ASP		白杨	41—65	89*	5.5	NA	成年的白杨，下垫面为榛树	(Deering，1999)

*表示冠层的郁闭度

被覆盖度(Defries 等，2000)，MODIS地表覆盖的物候期产品(Zhang 等，2003)

分析MODIS二向性反射角度指数产品，需要提取高质量和较纯的地表类型，以减少由于可能的亚像元云的影响和混合像元带来的不确定性。考虑到MODIS地表分类和地表覆盖度两个产品各自的特点，我们用这两种产品的交集，提取了一些较纯的国际地圈生物圈计划(IGBP)地表类型，然后根据MODIS二向性反射和反照率产品在相应波段的质量标志作为约束条件，获取最好质量的二向性反射模型参数和BRDF校正的天顶方向的反射率产品。

本研究采用三个约束条件来提取高质量的MODIS/BRDF参数样本数据：(1)给定所选的MODIS二向性反射参数具有最好的质量(质量标志为0)，即MODIS二向性反射参数的质量标志的优先级最高，以保证所选用的样本BRDF的质量最可靠；(2)对应像元的MODIS覆盖度的值大于70%；(3)对应像元MODIS地表IGBP类别有较高的置信水平。通过以上3个限制条件和对研究区的常绿针叶林和农作物两大类别进行等间隔重采样，最终使研究区的7个选中类别的样本像元数保持在每类100个像元左右(表3)。

表3 实验区MODIS样本像元，要求MODIS的IGBP类别有高置信度，MODIS二向性反射和反照率产品有最好的质量以及MODIS覆盖度产品有较高的丰度

地表覆盖类型(IGBP)	类型编号	类标志	置信度/%	像元样本
常绿针叶林	ENF	1	=100	101
混合林	MF	5	=100	144
稀疏灌木林	OS	7	≥76	101
稀树大草原	WS	8	≥83	100
草地	GL	10	≥99	143
农作物	CL	12	=100	101
农作物和自然植被混合类	CNVM	14	≥97	119

4 基于地表观测数据分析MODIS二向性反射角度指数

4.1 地表观测数据的二向性反射角度指数计算

在基于互易的RossThick-LiSparse-Reciprocal (RTLSR)模型基础上，首先用AMBRALS程序反演出地表20组BRDF观测的三个模型参数。AMBRALS程序是一套基于多核思想，面向用户的半经验、核驱动模型的程序集，其中包含了MODIS二向性反射和反照率算法中所用的罗斯表层核和李氏稀疏互易核，因此和MODIS在轨运行业务化的RTLSR算法有一定程度的兼容。然后，利用核权重系数直接构造，或通过参数计算典型散射角(热点、天顶和冷点方向)的反射率，然后进一步计算MODIS二向性反射角度指数。计算中采用均方根误差(RMSE)来衡量模型的拟合能力。均方根误差可用式(3)表示:

$$e^2 = \frac{1}{N - n_p} \sum_{j=1}^{N} \frac{(R_j^{\text{obs}} - R_j^{\text{model}})^2}{W_j} \tag{3}$$

式中，N是观测数，n_p是模型的参数个数，R_{obs}和R_{model}分别是观测和模型的反射。W_j是权重因子，用来权重不同的观测。在缺乏先验知识的情况下，W_j通常被指定为1。

这20组多角度观测数据在红和近红外波段的均方根误差都小于0.1，它们的平均均方根误差约为0.0142和0.0312，表明RTLSR模型对这些数据系有较好的拟合。0.1的域值是根据MODIS BRDF/Albedo的质量控制条件给出(Jin 等，2003；Shuai 等，2008)。由计算可知，对于植被，近红外波段的绝对拟合误差比红波段的要稍大一些，但它们的相对误差差别不大，这可能与植被在红和近红外波段所表现出的不同的反射特征，以及模型对植被不同波段的拟合能力有关。

基于20组地表的BRDF观测，我们计算了MODIS的二向性反射角度指数随不同植被类型的变化(图2)。对比图2的ANIF和ANIX可以看出，在红和近红外波段都有ANIX>ANIF>1。由此，我们基本可以判断出这20组观测的BRDF基本形状为：后向45° 的反射，大于天顶方向的反射，大于前向45° 的反射。这些观测BRDF形状的共同特点就是后向散射大于前向散射。但具体可能是何种BRDF形状，我们无法从ANIF和ANIX给定的域值进行判断。因此，基于典型散射角的二向性反射角度指数虽然在某种程度上指示了地表各向异性反射的一些信息，但对于

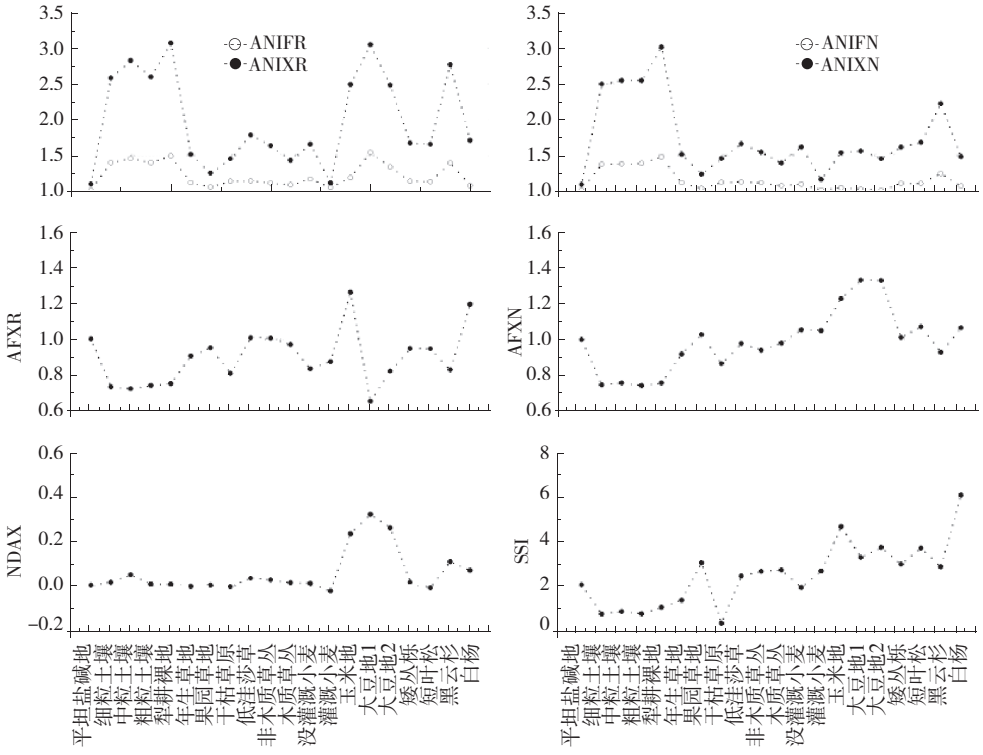

图2 地表20组BRDF观测计算得到的MODIS的各向异性角度指数

识别完整的BRDF形状时，存在着局限性。以前关于ANIF和ANIX的文献分析，多数集中在BRDF的光谱效应的分析上，对它们指示BRDF形状的能力缺少分析。

从图2的两条AFX曲线中，我们也可以看出AFX的值围绕着1变化。这种变化是由几何光学和体散射两种基本散射类型的相对大小决定的，这种变化与基本的BRDF形状的关系，我们将会进一步的分析。NDAX和SSI复合了红和近红外波段的光谱信息，它们对特定波段的BRDF形状的指示意义不明显。

4.2 基于地表观测数据的模型参数分析

如前所述，MODIS二向性反射角度指数的构造依赖于半经验、核驱动的二向性反射模型，因此，分析模型参数在这20组BRDF观测中的变化，有助于理解MODIS二向性反射角度指数。我们统计了20组地表观测所反演的模型参数的均值，方差和变异系数(表4)。

表4 利用地表20组BRDF观测反演得到的体散射和几何光学参数在红和近红外波段的统计

参数类型	均值	方差	变异系数
VOL_Red	0.0601	0.0527	0.8759
GEO_Red	0.0248	0.0271	1.0928
VOL_NIR	0.1869	0.1202	0.6433
GEO_NIR	0.0303	0.0324	1.0673

由表4可以看出，在红和近红外波段，几何光学参数的均值很接近，体散射参数明显大于几何光学参数。从它们的变异系数可以看出，几何光学参数相对于体散射参数表现的更为离散。从体散射参数和几何光学参数的大小看，在近红外波段，体散射参数明显占主导地位，几何光学参数在红波段和近红外波段大小相近。因为在核驱动模型中，体散射通常理解为由冠层内随机分布组份的间隙率引起的多次散射，而几何光学散射通常可理解为多个树冠的间隙率引起的单次散射。因此，几何光学参数和体散射参数相比更离散，可能表明了树冠内和树冠间的间隙率的分布存在有意义的差异。

我们计算了体散射和几何光学参数的决定系数(R^2)(表5)，它定义为相关系数的平方。我们首先分析模型参数在不同波段之间的相关性。由表5可以看出，几何光学参数在原始的红和近红外波段的决定系数约为0.84，而体散射参数在红和近红外波段的决定系数仅为0.022，表明这两个波段的体散射参数能提供更为独立的地表散射信息，因此，在分析地表属性时，红和近红外波段的体散射参数比几何光学参数可能会更有用。对于同一波段的两个参数的相关性，在红波段，几何光学参数和体散射参数的相关性较高(决定系数约为0.6)，而对于近红外波段，几何光学参数和体散射参数几乎不相关，它们的决定系数为0.083，这表明近红外波段的体散射和几何光学参数能提供较为独立的地表散射的信息，它们对分析地表特性可能会更有用。

表5 原始的体散射和几何光学参数的决定系数(R^2)

	VOL_Red	GEO_Red	VOL_NIR	GEO_NIR
VOL_Red	1.0000	—	—	—
GEO_Red	0.5856	1.0000	—	—
VOL_NIR	0.0220	0.0054	1.0000	—
GEO_NIR	0.5795	0.8435	0.0833	1.0000

4.3 MODIS角度指数之间的相关性

我们计算了MODIS二向性反射角度指数之间的决定系数，以确定各角度指数之间是否存在明显的信息冗余。表6是MODIS角度指数之间的决定系数。由表6可以看出，对同一波段之间，ANIF和几个角度之间存在着较为明显的相关，例如，相同波段的ANIF和AFX之间的决定系数约为0.5—0.65，相同波段的ANIF和ANIX之间的相关最为明显，它们的决定系数大于0.9，这说明ANIF和ANIX存在显著的数据冗余。因此，我们建议在MODIS二向性指示因子产品中去掉ANIF，这将有助于减少MODIS二向性反射角度指数产品的数据量，但对于产品的应用可能不会产生大的影响。

表6 MODIS二向性反射角度之间的决定系数

	ANIFR	ANIFN	ANIXR	ANIXN	AFXR	AFXN	NDAX	SSI
ANIFR	1.000	—	—	—	—	—	—	—
ANIFN	0.435	1.000	—	—	—	—	—	—
ANIXR	0.916	0.387	1.000	—	—	—	—	—
ANIXN	0.607	0.944	0.592	1.000	—	—	—	—
AFXR	0.501	0.267	0.229	0.274	1.000	—	—	—
AFXN	0.027	0.659	0.007	0.429	0.104	1.000	—	—
NDAX	0.221	0.078	0.323	0.007	0.000	0.519	1.000	—
SSI	0.096	0.374	0.015	0.235	0.475	0.542	0.216	1.000

表7 MODIS二向性反射角度指数和NDVI的决定系数(R^2)

	ANIFR	ANIFN	ANIXR	ANIXN	AFXR	AFXN	NDAX	SSI
NDVI	0.012	0.325	0.001	0.175	0.200	0.589	0.366	0.829

4.4 MODIS二向性反射角度指数和光谱指数之间的相关性

我们计算了MODIS的几个角度指数和归一化植被指数(NDVI)之间的决定系数(R^2)，以分析各向异性角度指数相对于NDVI的信息量。NDVI是通过红和近红外波段的反射差异性，经归一化处理构造而成，它通常用来度量植被光合作用的能力强弱，具有下列简单的形式：

$$\mathrm{NDVI} = (R_{\mathrm{NIR}} - R_{\mathrm{red}}) / (R_{\mathrm{NIR}} + R_{\mathrm{red}}) \quad (4)$$

式中，R_{NIR}和R_{red}分别表示在红和近红外波段的反射率。在此，NDVI是利用MODIS的NBAR产品(二向性反射纠正的反射率)进行计算，因此，NDVI是一个光谱量，不包含与二向性反射有关的信息。由表7可以看出，总的说，MODIS二向性反射角度指数和NDVI之间有较小的决定系数，说明MODIS的二向性反射角度指数包含着与NDVI不同的信息含量。

对于SSI与NDVI之间的关系，Gao 等(2003)已进行过较为详细的探讨，在此我们采用了类似的方法，分析了AFX和NDVI的关系，重点分析AFX有不同于光谱指数NDVI的信息含量，及AFX随着两种基本散射类型的变化对地表二向性反射模式的指示作用。对于其他的几个角度指数也可以进行类似的分析。

图3表示了红和近红外波段的AFX与NDVI之间的散点图。从图3可以看出，各向异性平整指数和归一化植被指数的线性关系不明显，说明NDVI和AFX有不同的信息含量。基本上，大的AFX的值对应于大的NDVI的值。这说明AFX和NDVI有相似的地方，都可能和植被的生物量有关系。但AFX相对于NDVI的变化表明，AFX不同于NDVI，它实际上按照地表的各向异性的散射模式指示着地表目标的变化。在NDVI的中间值范围内(0.3—0.7)，AFX接近于1，但在NDVI的低端(0—0.3)和高端(0.7—1.0)这两个范围内，相近的NDVI值对应的AFX的值有更多的变化。例如，在近红外波段，在NDVI的低端，小麦(CUW)的AFX的值要比土壤(S2、S3、S4和S5)和稀疏的草地(GS和GA)大。在NDVI的高端，大豆(CS1和CS2)和小麦(CIW)的AFX的值要比森林(OBS、OJP和ASP)的AFX的值大，这是因为农作物的播种期基本一致，因此常常表现出比森林和粗糙的土壤更为均匀和缺少聚集性。这种结构的差异决定了农作物在近红外波段的体散射效应更为明显。在红波段，农作物，尤其大豆的垄行结构(Ranson 等，1985)使几何光学效应更加显著。图3说明了AFX可以在某种程度上反映出植被结构的三维信息，这是NDVI所不具备的。

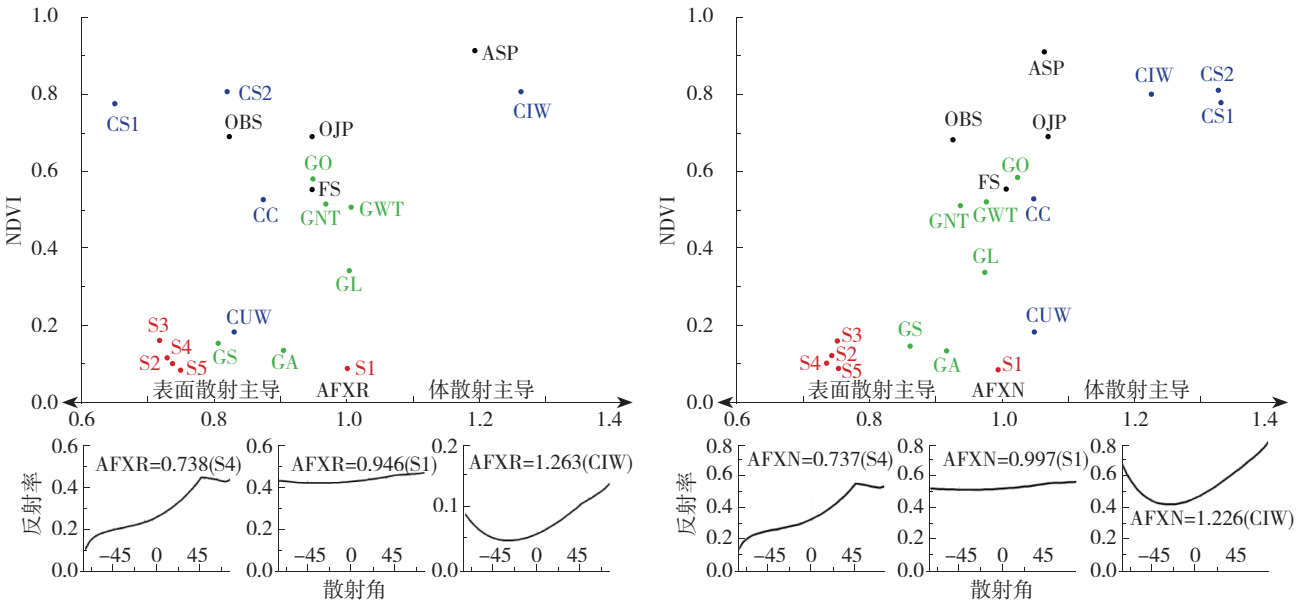

图3 基于地表20组BRDF观测，红和近红外波段的AFX和天顶观测的NDVI的散点图(下方的3个小图分别表示主平面上3个典型地物的BRDF形状: 粗糙土壤，平坦的盐碱地及浓密的小麦地；3个小图的横坐标的正轴方向代表后向散射方向，负轴方向代表前向散射方向；太阳的天顶角为后向45°)

图3底部的三个小图表示了在主平面方向上，3种地物类型：粗糙土壤，平坦的盐碱地及长势茂密的小麦的BRDF形状的差异。从这3个图看出，粗糙的土壤在主平面上呈现典型的屋顶状，这个屋顶状在后向散射的热点方向上有一个明显的峰值，此时AFX<1；对于平坦的盐碱地，BRDF的形状相对平整，指示着该地物类型更接近一个朗伯表面，此时的AFX≈1；对于茂密的小麦地，体散射类型主导着该种地物类型，辐射传输理论此时可能更适合对这种地物类型的描述，因此，它表现为一个碗状的BRDF形状，此时AFX>1。由以上分析可以看出，AFX对BRDF形状有较好的指示作用，并且和地表的结构有关。

从AFX的构造方式上，我们可以看出，AFX通过拟合可获得的二向性观测，得到关于地表二向性反射的整体信息，并去除了地表各向同性的影响，因此，AFX可能提供关于地表各向异性反射更为完整的描述。我们可以根据它的值的大小，更好的刻画BRDF的形状。其他的角度指数，如ANIX，利用BRDF形状的两个典型散射角的反射进行构造，这种构造方式并没有考虑所有可能的二向性观测。AFX是根据几何光学效应和体散射效应的相对量大小，决定地表实际的散射类型，因此物理意义更为明确。

4.5 MODIS二向性反射角度指数的光谱效应

根据二向性反射角度指数在红和近红外波段不同的表现，我们进一步分析BRDF的光谱效应。Kimes(1983)和Sandmeier 等(1998)对BRDF光谱效应的机制已经进行了较为完整的分析，认为BRDF的光谱效应主要由地表的结构特性，地表组份的散射特性及它们的相互作用引起的。在此，我们主要针对构成核驱动BRDF模型的两种基本散射类型：几何光学效应和体散射效应相对量的大小做定性的分析。由图4可以看出，ANIX在红波段的值大于近红外波段的值，对于植被尤为明显，而对于AFX来说正好相反，是近红外波段的值大于红波段的值，同样对于植被类型显著。和土壤表面的散射相比，植被冠层在红和近红外波段的散射表现出更大的差异。因此，MODIS角度指数在光谱波段的差异性可能与不同地表类型的散射有关。

在红光波段，由于植被叶绿素的强吸收使单次散射增强，使植被在该波段的几何光学效应增强；而在近红外波段，由于叶子的高透射使多重散射效应增强，因而增加了体散射效应在近红外波段的影响。根据体散射和几何光学核的形状(图1)可以看出，对于几何光学散射为主的地表类型，BRDF形状在热点和冷点的对比明显；而对于体散射效应为主的地表类型，BRDF形状在热点和冷点的反射对比要稍弱一些。因此，ANIX作为各向异性散射在热点和冷点反射率的比值，一般表现的在红光波段要大于近红外波段。但AFX描述的是几何光学和体散射的相对强弱，对于几何光学效应相对较强的红波段，AFX的值通常小于1，对于体散射效应相对较强的近红外波段，AFX的值通常大于1(图4)。因此，二向性反射角度指数在红和近红外波段的差异，实际上是由几何光学效应和体散射效应在这两个波段的相对量的大小决定的。

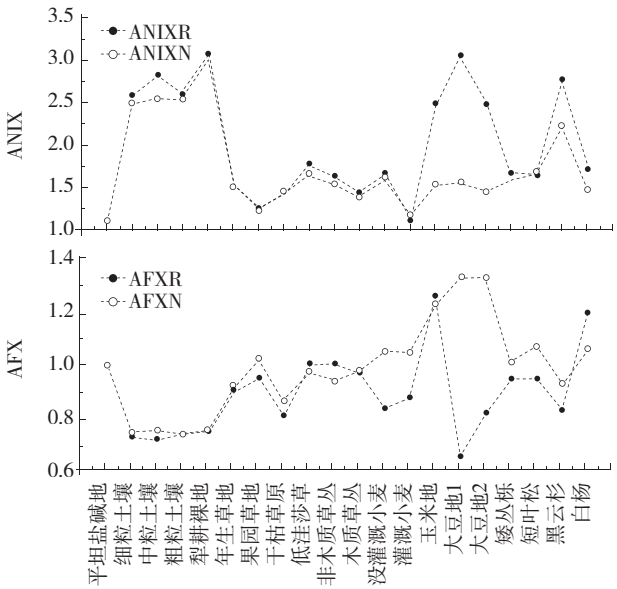

图4 地表20组观测的红和近红外波段的ANIX和AFX

5 基于MODIS采样数据分析角度指数产品

如前所述，MODIS的二向性反射角度指数，一部分是借鉴已有的角度指数的构造形式，如ANIF、ANIX及NDAX。这些角度指数最早是用来分析典型植被的BRDF光谱效应，并发现它们和植被的结构有关。对于MODIS传感器而言，这3个角度指数只有借助核驱动的BRDF模型才能构造。这是因为对于MODIS传感器，它的多角度的获取方式和采样能力使它很难获得典型散射角度(如热点和冷点)的反射

(Barnsley 等，1994)，因此，需要用星载采样数据对这些角度指数做进一步的分析。AFX和SSI是基于MODIS的BRDF模型参数构造的各向异性指数。SSI已基于地表的BRDF观测及星载的MODIS和MISR的采样(Gao 等，2003)进行了系统完整的分析，但对AFX缺乏类似完整的分析。这部分我们将重点基于星载的MODIS采样数据来分析这些角度指数。

5.1 用MODIS采样数据对角度指数进行相关计算和主成分分析

我们用选中的MODIS样本数据(表2)，对MODIS的二向性反射角度指数进行了相关计算和主成分分析。由于云的影响，我们从实验区中选用了2004年4个时相(177，193，257和273儒略日)的角度指数产品，并计算了它们之间的决定系数(R^2)(表8)。从表8可以看出，对于MODIS的采样样本，ANIF和ANIX的相关性仍然很高，其决定系数约为0.9。这表明去掉ANIF指数对使用这些角度指数可能不会产生有意义的影响，这一分析和基于地表观测数据的结果基本是一致的。

表8 MODIS二向性反射角度指数的决定系数(R^2)

	ANIFR	ANIFN	ANIXR	ANIXN	AFXR	AFXN	NDAX	SSI
ANIFR	1.000	—	—	—	—	—	—	—
ANIFN	0.134	1.000	—	—	—	—	—	—
ANIXR	0.933	0.149	1.000	—	—	—	—	—
ANIXN	0.158	0.867	0.192	1.000	—	—	—	—
AFXR	0.535	0.050	0.314	0.039	1.000	—	—	—
AFXN	0.059	0.711	0.057	0.399	0.043	1.000	—	—
NDAX	0.587	0.031	0.604	0.023	0.279	0.027	1.000	—
SSI	0.112	0.153	0.064	0.050	0.280	0.303	0.030	1.000

为了对MODIS二向性反射角度指数的内在维数有进一步的了解，我们对这4个时相的MODIS采样数据进行主成分分析。主成分分析通过一个线性变换，将有待分析的变量变换到几个相互正交的轴上，称之为主成分，因此，各主成分之间不相关。利用主成分分析技术，我们可以分析出这几个角度指数的相互关系和前几个主成分可能代表的物理意义。在此，我们同样对选中的四个时间的MODIS角度指数的样本数据进行主成分变换，得到特征根和每个特征向量可解释方差的百分比(表9)。因为这些角度指数在表征地表的各向异性反射时，有不完全相同的意义，所以在进行主成分变换时，我们应用这些角度指数的相关阵来计算不同的主成分。

从表9可以看出，前3个主成分的方差之和占总方差的百分比大于90%，说明MODIS各向异性角度指数所包含的信息量可近似为内在3维。表10描述了MODIS角度指数的每个成分的权重系数。因为前3个主成分解释了这些角度指数的绝大部分方差，所以，我们主要解释前3个主成分可能的意义。

表9 MODIS二向性反射角度指数的特征根及每个特征向量可解释的方差百分比

特征向量	特征根	可解释方差百分比/%
1	3.9533	49.4161
2	2.3517	29.3957
3	0.9937	12.4218
4	0.4051	5.0638
5	0.2165	2.7058
6	0.0601	0.7517
7	0.0150	0.1879
8	0.0046	0.0572

由表10第1个特征向量可以看出，这些角度指数在第一个特征向量中的权重系数相差不大，其中红波段的角度指数的权重系数要稍大一些，说明红波段在第一主成分中有更大的贡献。从第一主成分权重系数的正负号，我们可以将MODIS的二向性反射角度指数分为两类：基于典型散射角反射率的角度指数和基于模型参数的角度指数，这两组指数表现为负相关。基于反射率的角度指数包括ANIF，ANIX和NDAX，在第1组特征向量中，表现为负的权重系数。而基于模型参数的角度指数包括AFX和SSI，在第一组特征向量中表现为正的权重系数。这两组角度指数的负相关关系，我们可以从它们的表达式得到解释。

表10 MODIS各向异性角度指数的主成分权重系数

PC轴	ANIFR	ANIFN	ANIXR	ANIXN	AFXR	AFXN	NDAX	SSI
PC1	−0.444	−0.357	−0.4273	−0.336	0.361	0.311	−0.254	0.297
PC2	0.273	−0.440	0.2523	−0.382	−0.229	0.426	0.529	0.092
PC3	−0.165	−0.164	−0.3121	−0.374	−0.350	−0.182	−0.049	−0.742
PC4	0.036	0.024	−0.2265	0.267	−0.732	0.394	−0.370	0.220
PC5	−0.039	0.001	0.1129	0.398	0.316	0.653	−0.040	−0.547
PC6	−0.521	0.242	−0.3096	0.253	−0.138	0.039	0.696	0.075
PC7	0.134	0.767	−0.0778	−0.531	0.045	0.323	−0.018	0.002
PC8	−0.640	0.067	0.7003	−0.159	−0.197	0.031	−0.174	0.010

由表1中的ANIF、ANIX、NDAX和SSI的表达式和式(2)可以推断出，对于某种地表类型，SSI和AFX随着体散射效应的增强而明显变大。通过对MODIS各向异性散射模式的分析可知，以体散射效应为主的地表类型，它们的BRDF的形状常常表现为一前向倾斜的碗状，而以几何效应为主的地表类型，它们的BRDF形状常常表现为后向散射有较强热点的屋顶状。随着地表的主要散射类型从几何光学效应到体散射效应的过渡，其各向异性散射模式的热点与冷点的对比有减小的趋势，因此，基于热点和冷点反射比构造的ANIX有下降的趋势，由于ANIF和ANIX高相关，所以ANIF也呈现下降趋势。NDAX是红和近红外波段归一化的ANIX，也基本呈现出下降的趋势。由以上分析可知，随着地表主要散射类型从几何光学到体散射类型的变化，基于反射率的MODIS角度指数和基于模型参数的MODIS角度指数是负相关的关系，这与第1主成分分析代表的意义是一致的。

分析第2特征向量的权重系数我们可以看出，近红外波段比红波段有更大的权重，且红和近红外波段也呈现出负相关关系，表明第2主成分主要反映了ANIF，ANIX和AFX这3个角度指数在红和近红外波段的光谱之间的差异。不同于植被在红和近红外光谱反射率的差异，这3个角度指数的波段差异主要反映了BRDF的形状在这两个波段的不同，它反应了BRDF的光谱效应的差异。对于MODIS的各向异性散射模式，红光波段几何光学效应常常大于体散射效应，使红波段的各向异性散射模式常常表现为一个后向有反射峰值的屋顶状。在近红外波段，多重散射效应增强，尤其对于连续的植被结构，各组分间的多重散射增强了体散射效应，使近红外波段的各向异性散射模式常常表现为一个碗状的BRDF形状。由以上分析可以看出，由于植被结构和主要散射类型的变化，在红和近红外波段，植被常常呈现出不同的各向异性散射模式，这与主成分分析的第2特征向量所代表的意义是一致的。

对于第3个特征向量，SSI的权重系数最大，且所有的系数都为负值，说明各角度指数对第3主成份有相同类型的贡献。由于MODIS角度指数是借助于地表的各向异性散射模式构造，而各向异性散射和地表类型的结构有关，所以，第3个特征向量可能是和植被结构有关的主成分。由表9可知，第3个主成分约占总方差的12%，表明第3主成分在识别地物目标信息时可能提供较为次要的信息量。如果第3主成分只和植被结构有关，那么植被结构所能提供的信息量虽然并不占主导，但确实提供了额外的信息含量。

5.2 分析MODIS角度指数类内方差的变化

基于选中的MODIS样本数据(表2)，我们对实验区的几个典型地表类型进行类内方差的统计，这对研究应用角度指数来提高地表分类精度有重要的意义。Sandmeier和Deering(1999)以及Bicheron和Leroy(2000)认识到对于同种植被类型，各向异性指数(ANIX)存在较大的类内方差。然而，他们并没有进一步分析方差随波段变化的规律。本研究采用选中的MODIS样本数据，以ANIX和AFX为例，计算了这些样本的均值、方差及变异系数，分析了各向异性角度指数在红波段及近红外波段的方差的变化规律。变异系数定义为标准差与均值的比值，它消除了单位和(或)平均数不同对两个或多个资料变异程度比较的影响。

图5显示了两个典型的MODIS各向异性角度指数ANIX和AFX在近红外和红波段的均值、方差和变异系数。对比ANIX和AFX可以看出，这两个角度指数在红和近红外波的均值变化趋势表现出负相关。对于ANIX，红波段的值大于近红外波段的值，对于AFX，近红外波段的值大于红波段的值，这和主成分分析的第1个特征向量的结果是一致的。正如前面分析，它们光谱效应差别的物理机制是由几何光学散射效应和体散射效应共同作用的结果，并与地表的结构有关。

结合选用的7个IGBP类型的特点，对图5中各种植被类型均值变化做进一步的分析。该研究所用的植被类型基本可以分为两大类：具有离散结构的森林和具有连续结构的草本植被。森林植被类型，以常绿针叶林的结构表现最为典型，对于常绿针叶林，其组分的等级结构决定了它们有明显的聚集效应，从松针到针簇，到簇团，到树枝，再到树冠，由树冠形成了不同密度的林地，最后达到景观尺度。针叶林的这种非随机和等级式的聚集结构，决定了后向阴影效应可能控制着这种植被类型。从构成核驱动模型的几种基本的散射类型来讲，这种聚集结构通常决定了该植被类型可能以几何光学效应为主。相反，对于连续的草本植被，如草原和农作

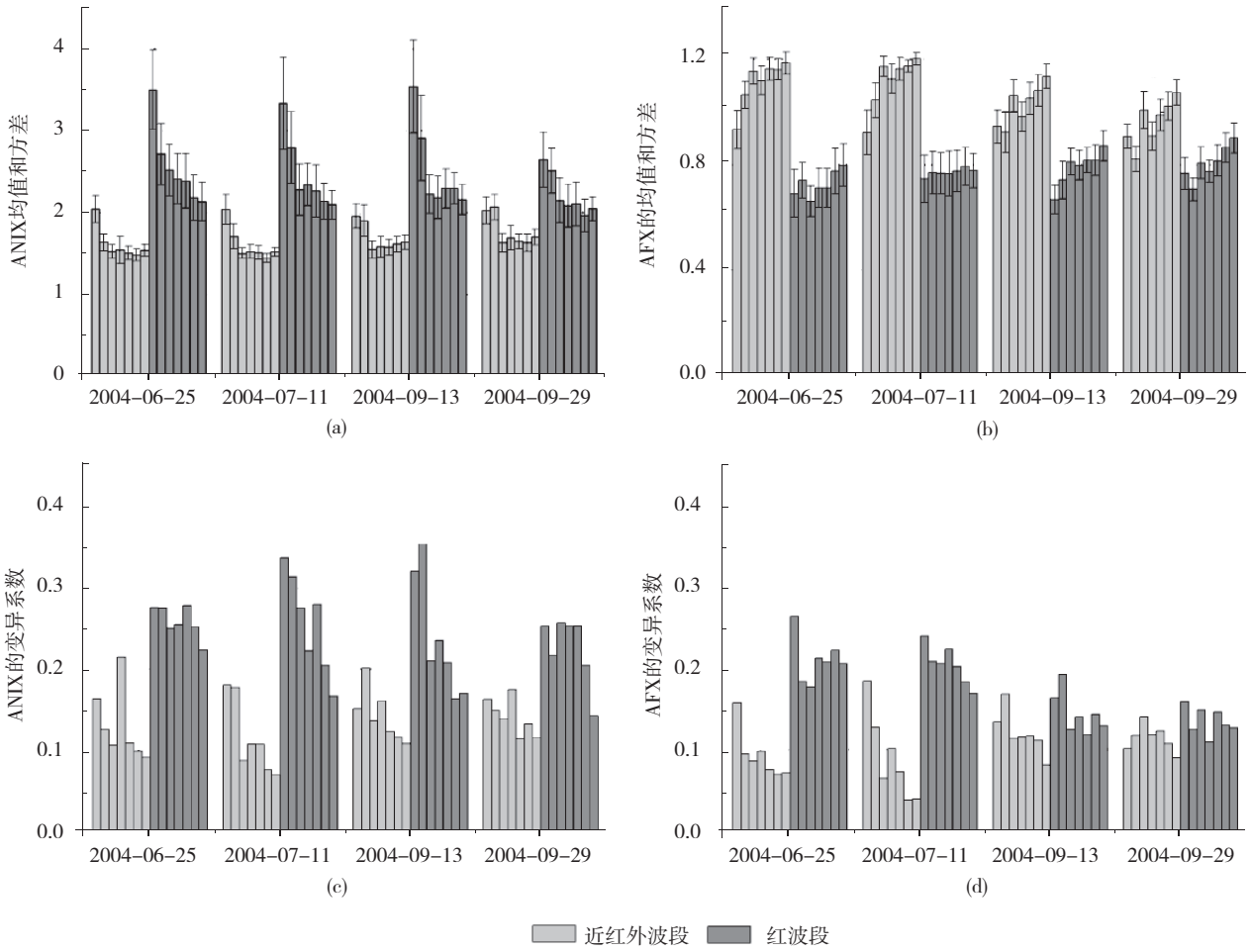

图5 (a)和(c)为ANIX在近红外波段和红波段的均值，方差和变异系数；(b)和(d)为AFX在近红外波段和红波段的均值，方差和变异系数(图中的横坐标表示不同的物候期，浅灰色的柱群表示近红外波段，灰色的柱群表示红波段；每个日期中的7个小柱条依次代表了IGBP分类体系中的长绿针叶林(ENF)，混合林(MF)，稀疏灌木林(OS)，稀树大草原(WS)，草地(GL)，农作物用地(CL)，农作物和自然植被镶嵌地(CLVM)；(a)和(b)两图中的误差柱代表一个标准差；(b)图中的横实线代表在AFX=1时，各地表类型更接近朗伯散射)

物等，它们的结构通常可以假设为随机分布，对于这样一种植被结构，辐射传输的建模方法更适合这种植被类型。我们知道，李氏稀疏互易几何光学核的基本形状是一个后向散射有峰值的屋顶状，而罗斯表层核体散射核的形状是一个前向倾斜的碗状。因此，我们用这两个核拟合实际观测时，得到的BRDF形状也常为这两个形状的复合。而这两个典型的BRDF形状，通常与不同的波段有关，取决于不同波段对太阳辐射的吸收和散射的大小，这也是由几何光学散射和体散射的光谱效应决定的。

考察图5不同植被类型在红和近红外波段的方差变化可以看出，相对于近红外波段，红波段有更离散的方差，它们的变异系数更明显地表明了这一点。从图5这两个角度指数的变异系数可以看出，不同植被类型的变异系数在红波段比近红外波段大，表明在红波段方差相对于均值更离散。比较ANIX和AFX两种角度指数的变异系数可以看出，AFX比ANIX有更小的类内方差，说明AFX对于识别不同的地表类型可能会提供更有效的信息。

为了考察几何光学与体散射两种基本散射类型随不同植被类型的变化，及对同一植被类型随不同时间的变化，我们计算了对应于实验区MODIS样本数据的植被物候期数据的均值(表11)。由表11可以看出，实验区中这7种植被类型的物候期相差不大，一般从5月中旬前后植被开始变绿，6月底至7月中旬，植被绿度达到最大值，8月中下旬，植被绿度开始下降，9月底至10月初，植被绿度降至最小。

表11 MODIS采样数据的物候期均值

	OGI	OGmax	OGD	OGmin
ENF	05–18	07–08	08–23	09–26
MF	05–17	06–27	08–25	10–03
OS	05–22	07–12	08–30	10–04
WS	05–20	07–03	08–26	10–03
GL	05–20	07–10	08–28	10–05
CL	05–20	07–17	08–23	10–05
CNVM	05–11	07–15	08–18	10–08

注：OGI, OGmax, OGD, OGmin指绿度开始增加(Onset of Greenness Increase)，绿度最大值的开始(Onset of Greenness Maximum)，绿度降低的开始(Onset of Greenness Decrease)和绿度最小值的开始(Onset of Greenness Minimum)，单位为(月−日)。ENF, MF, OS, WS, GL, CL和 CNVM所代表的类型与图7相同。

由前面的分析可知，几何光学和体散射两种基本散射类型的相对量的大小决定了AFX值围绕着单位1变化。对于MODIS采样数据，由图5可以看出，在红波段，所有的植被类型，在不同的时间，都有AFX小于1，表明它们由几何光学散射类型为主，指示着一个屋顶状的BRDF形状。在近红外波段，对于不同的植被类型，几何光学和体散射随着时相变化交互发生变化。具体分析，在4个所示的时相上，常绿针叶林的几何光学效应大于体散射效应，从而有AFX<1；农作物类型和农作物/自然植被镶嵌类型，体散射效应大于几何光学效应，从而有AFX>1。其他的植被类型，包括混合林、稀疏灌木林、稀树大草原和草地，在绿度最大时期，由于体散射效应大于几何光学效应，使AFX>1；在衰落期，由于植被叶子的减少，使体散射减少而后向阴影效应显著，导致几何光学效应大于体散射效应，从而有AFX<1。从植被结构来看，常绿针叶林具有典型的不同级别的聚集结构，农作物的各组分通常可假设为随机分布，混合林等其他类型处于两者的过渡带，并随时间的变化而改变。因此，我们可以看出，AFX与不同植被类型的结构有关，并随着时相而变化。因此，我们有可能通过AFX来区分不同结构的植被类型，以及探索这些植被结构的时相变化情况。

6 结 论

MODIS的二向性反射角度指数是基于半经验、核驱动的BRDF模型，针对地表的各向异性散射模式构造而成。本研究利用地表BRDF数据系及星载的MODIS采样数据，对MODIS的二向性反射角度指数产品进行了较为系统的比较研究。通过分析可以看出，MODIS的二向性反射角度指数不同于光谱指数(如NDVI)，它们含有与植被结构有关的信息量，因此有可能通过它们来提取地表的结构信息。通过对地表测量数据及星载采样数据的相关分析表明，在红和近红外波段的各向异性因子(ANIF)和各向异性指数(ANIX)有较高的相关性，考虑到各向异性指数(ANIX)在热点和冷点反射具有更大的动态范围和具有更好的代表性，我们建议去掉ANIF角度指数，这有利于精炼MODIS的角度指数产品，但对利用这些角度指数产品可能不会有大的影响。

通过对MODIS的二向性反射角度指数进行主成分分析，得出MODIS的二向性反射角度指数基本是内在 3 维，解释了各主成分所可能表示的意义。这一分析类似对多光谱信号的主成分分析，由于第 3 个主成分是来自各角度指数相同类型的贡献，因此可能主要是一个和地表结构有关的量，它解释了总方差约10%的信息量。

我们进一步研究了BRDF形状和AFX的关系，发现AFX的变化与两种基本散射类型的相对大小有关，较好地指示着BRDF的形状的变化：AFX < 1表示几何光学散射类型为主导，指示着一个屋顶状的BRDF形状，该形状常常在后向散射方向有一个热点峰值；AFX > 1表示体散射效应为主导，指示着一个碗状BRDF形状，其特点是天顶方向的反射率小于大散射角反射率的值；AFX≈1指示着一个较平的BRDF形状。AFX随着波段和时相而变化，并和不同地表类型与地表结构有关。

通过分析MODIS二向性反射角度指数的方差随地表类型及波段的变化规律，发现这些角度指数在红波段比近红外波段有更为离散的方差，而对同种地表类型，AFX类内方差小于ANIX。因此，AFX作为光谱信号的补充信号在改善地表分类精度等方面可能会优于ANIX。

MODIS二向性反射角度指数产品现在是MODIS二向性反射产品的一个重要组成部分，随着业务化的MODIS BRDF和反照率产品的不断升级，以及国内外计划发射的新型的环境卫星系统如NPOESS(National Polar-orbiting Operational Environmental Satellite System)，本研究成果将会对这些星载传感器如何利用和构造各向异性角度指数，以拓展地表各向异性反射模式的应用，具有现实指导意义和实际应用价值。

MODIS二向性反射角度指数只对MODIS BRDF/Albedo算法的全反演(full inversion)有效。因此，对于16d一个周期累积的二向性反射产品，由于云和大气气溶胶的影响，虽然目前已复合了Terra和Aqua的两个传感器的观测数据，但常常很难获得区域和时间序列上一个完整的MODIS二向性反射的全反演数据，这为大区域和长时间序列地应用MODIS的二向性反射角度指数(如在区域和全球分类产品中的应用)带来了较大的困难。一个解决办法是通过复合时相序列的二向性反射产品以产生高质量的MODIS角度指数产品，这是今后研究MODIS角度指数产品的一个可能方向。

REFERENCES

Barnsley M J, Strahler A H, Morris K P and Muller J P. 1994. Sampling the surface bidirectional reflectance distribution function (BRDF): evaluation of current and future satellite sensors. *Remote Sensing Review*, **8**: 271–311

Bicheron P and Leroy M.2000. Bidirectional reflectance distribution function signatures of major biomes observed from space. *Journal of Geophysical Research*, **105** (D21): 26669–26681

Deering D W, Eck T F and Banerjee B. 1999. Characterization of the reflectance snisotropy of there boreal forest canopies in spring-summer. *Remote Sensing of Environment*, **67**: 205–229

Deering D W, Eck T F and Grier T. 1992. Shinnery oak bidirectional reflectance properties and canopy model inversion. *IEEE Transactions on Geoscience and Remote Sensing*, **30** (2): 339–348

Deering D W, Eck T F and Otterman J. 1990. Bidirectional reflectances of three desert surfaces and their characterization through model inversion. *Journal of Agricultural and Forest Meteorology*, **52**: 71–93

Defries R S, Hansen M C, Townshend J R G, Janetos A C and Loveland T R. 2000. A new global 1-km dataset of percentage tree cover derived from remote sensing. *Global Change Biology*, **6**: 247–252

Friedl M A, McIver D K, Hodges J C F, Zhang X Y, Muchoney D, Strahler A H, Woodcock C E, Gopal S, Schneider A, Cooper A, Baccini A, Gao F and Schaaf C. 2002. Global land cover mapping from MODIS: algorithms and early results. *Remote Sensing of Environment*, **83**: 287–302

Gao F, Schaaf C B, Strahler A H, Jin Y and Li X. 2003. Detecting vegetation structure using a kernel-based BRDF Model. *Remote Sensing of Environment*, **86**: 198–205

Hu B, Lucht W, Li X and Strahler A H. 1997. Validation of kernel-driven semiempirical models for the surface bidirectional reflectance distribution function of land surfaces. *Remote Sensing of Environment*, **62**: 201–214

Irons J R, Campbell G S, Normal J M, Graham D W and Kovalick W M. 1992. Prediction and measurement of soil bidirectional reflectance. *IEEE Transactions on Geoscience and Remote Sensing*, **30** (2): 249–260

Jin Y, Schaaf C B, Gao F, Li X, Strahler A H, Lucht W and Liang S. 2003. Consistency of MODIS surface bidirectional reflectance distribution function and albedo retrieval: Algorithm Performance. *Journal of Geophysical Research*. DOI: 10.1029/2002JD002803

Kimes D S. 1983. Dynamics of directional reflectance factor distributions for vegetation canopies. *Applied Optics*, **22**(9): 1364–1372

Kimes D S, Newcomb W W and Tucker C J. 1985 Directional reflectance factor distributions for cover types of Northern Africa. *Remote Sensing of Environment*, **18**: 1–19

Lucht W, Schaaf C B and Strahler A H., 2000. An Algorithm for the retrieval of Albedo from space using semiempirical BRDF Models. *IEEE Transactions on Geoscience and Remote Sensing*, **38** (2): 977–998

Nicodemus F E, Richmond J C, Hsia J J, Ginsberg W I and Limperis T. 1977. Geometrical Considerations and Nomenclature for Reflectance. Washington, D.C.: Institute for Basic Standards

Ranson K J, Biehl L L. and Bauer M E. 1985. Variation in spectral response of soybeans with illumination, view, and canopy geometry. *International Journal of Remote Sensing*, **6** (12): 1827–1842

Roujean J L, Leroy M and Deschamps P Y. 1992. A bidirectional reflectance model of the earth's surface for the correction of remote sensing data. *Journal of Geophysical Research*, **97**: 20455–20468

Roujean J L, Tanre D, Breon F M and Deuze J L.1997. Retrieval of land surface parameters from airborne POLDER bidirectional reflectance distribution function during HAPEX-Sahel. *Journal of Geophysical Research*, **102** (D10): 11201–11218

Sandmeier S R and Deering D W. 1999. Structure analysis and classification of boreal forest using airborne hyperspectral BRDF data from ASAS. *Remote Sensing of Environment*, **69**: 281–295

Sandmeier S R, Muller C, Hosgood B and Andreoli G. 1998. Physical mechanisms in hyperspectral BRDF data of grass and watercress. *Remote Sensing of Environment*, **66**: 222–233

Schaaf C B, Gao F, Strahler A H, Lucht W, Li X, Tsang T, Strugnell N C, Zhang X, Jin Y, Muller J P, Lewis P, Barnsley M, Hobson P, Disney M, Roberts G, Dunderdale M, Doll C, Entrmont R P, Hu B, Liang S, Privette J L and Roy D. 2002. First operational BRDF/Albedo nadir reflectance products from MODIS. *Remote Sensing of Environment*, **83**: 135–148

Shuai Y, Schaaf C B, Strahler A H, Liu J and Jiao Z. 2008. Quality assessment of BRDF/albedo retrievals in MODIS operational system. *Journal of Geophysical Research*. DOI:10.1029/2007GL032568

Vierling L A, Deering D W and Eck T F. 1997. Differences in arctic tundra vegetation type and phenology as seen using bidirectional radiometry in the early growing season. *Remote Sensing of Environment*, **60**: 71–82

Wanner W, Li X and Strahler A H. 1995. On the derivation of kernels for kernel-driven models of bidirectional reflectance. *Journal of Geophysical Research*, **100**: 21077–21090

Zhang X, Friedl M A, Schaaf C B, Strahler A H, Hodges J C, Gao F, Reed B C and Huete A. 2003. Monitoring vegetation phenology using MODIS. *Remote Sensing of Environment*, **84**: 471–475